catalysts

MDPI

Article

Microwave-Assisted Solvothermal Synthesis of Fe_3O_4/CeO_2 Nanocomposites and Their Catalytic Activity in the Imine Formation from Benzyl Alcohol and Aniline

Antonino Rizzuti [1], Maria C. Dipalo [1], Ignazio Allegretta [2], Roberto Terzano [2], Nicola Cioffi [3], Piero Mastrorilli [1], Matilda Mali [1], Giuseppe Romanazzi [1], Angelo Nacci [3] and Maria Michela Dell'Anna [1,*]

1 Dipartimento di Ingegneria Civile, Ambientale, del Territorio, Edile e di Chimica Politecnico di Bari, via Edoardo Orabona 4, 70126 Bari, Italy; antonino.rizzuti@poliba.it (A.R.); mdipalo1@jhu.edu (M.C.D.); p.mastrorilli@poliba.it (P.M.); matilda.mali@poliba.it (M.M.); giuseppe.romanazzi@poliba.it (G.R.)

2 Dipartimento di Scienze del Suolo, della Pianta e degli Alimenti, Università degli Studi di Bari "Aldo Moro", via Giovanni Amendola 165/A, 70126 Bari, Italy; ignazio.allegretta@uniba.it (I.A.); roberto.terzano@uniba.it (R.T.)

3 Dipartimento di Chimica, Università degli Studi di Bari "Aldo Moro", via Edoardo Orabona 4, 70126 Bari, Italy; nicola.cioffi@uniba.it (N.C.); angelo.nacci@uniba.it (A.N.)

* Correspondence: mariamichela.dellanna@poliba.it

Received: 1 October 2020; Accepted: 12 November 2020; Published: 14 November 2020

Abstract: Fe_3O_4/CeO_2 nanocomposites were synthetized by coating magnetite seeds of different morphologies (hexagonal, spheroidal, quasi-spherical) with ceria, in ethylene glycol as solvothermal solvent. The synthesis was performed in the presence of microwave irradiation aiming to overcome the common disadvantages proper of the classic solvothermal/hydrothermal procedure. The obtained nanocomposites were calcined at the optimum temperature of 550 °C. The structure of the new nanomaterials was carefully investigated by IR, XRD, SEM, EDS and TEM analyses. The nanocomposites resulted to be constituted by CeO_2 nanoparticles distributed onto Fe_3O_4 seeds, that kept their pristine morphology. The new materials were used as catalysts for imine synthesis from benzyl alcohol and aniline. The highest imine conversion rate was obtained with Fe_3O_4/CeO_2, which was synthesized from Fe_3O_4 nanoparticles (hexagonal) obtained by microwave hydrothermal procedure in the absence of any organic additive (polyvinylpyrrolidone, trisodium citrate dihydrate or oleic acid). The catalyst could be easily removed from the reaction mixture with the help of an external magnet, and it was recycled for at least five runs with increasing catalytic activity.

Keywords: Fe_3O_4/CeO_2 nanocomposites; cerium oxide; microwave-assisted solvothermal synthesis; imine synthesis; redox chemistry

1. Introduction

Ceria is an oxide of the most abundant rare-earth metal of the lanthanide series, having the unique feature to pass from +4 to +3 oxidation state based on the occurrences [1]; thus, ceria exists as CeO_2 containing also Ce_2O_3. CeO_2 nanoparticles have highly reactive surface area due to presence of oxygen vacancies in their structures, acting as free radical scavengers [2], and they are useful for several applications, such as, biomedical [3,4], biological [5], gas sensing [6], catalysis [7], energy production [8] and optical devices [9]. Nanoceria can be synthetized following several methods [3–5,10,11], i.e., by precipitation [12], green synthesis [13], hydrothermal [14,15], solvothermal [16], microwave-assisted [17,18] and sonochemical [19]

procedure, and the way of synthesis strongly influences the morphological properties, thus the activity and reactivity of the obtained nanomaterial [20,21]. In the field of catalysis, nanoceria has been used as efficient catalyst for aerobic oxidation reactions due to its oxygen storage capability [22], although its recovery at the end of the catalytic cycle cannot be carried out by simple filtration, because of its too tiny consistency [23]. A method to overcome this disadvantage is to anchor nanoceria to magnetite (Fe_3O_4) [24–30], rendering the whole material easy to be removed from the reaction mixture by using an external magnet. So far few types of magnetic Fe_3O_4/CeO_2 nanocomposites with core-shell structure have been synthetized [31–34] and some of them have the problem of iron leaching during catalysis, which can be overcome by the addition of an organic polymer layer (polysulfone) [32] or a silica interlayer. In details, Chen and co-workers [31] synthetized $Fe_3O_4/SiO_2/CeO_2$ with the precipitation method, followed by calcination at 500 °C, obtaining nanoparticles with mean diameter of 150 nm; Wei et al. [32] prepared Fe_3O_4/CeO_2 of ca. 200 nm in size with the solvothermal/hydrothermal method; Rossi and co-workers [34] were not able to coat nanoceria directly onto magnetite nanoparticles without using a SiO_2 interlayer, and, finally, very small core-shell magnetite/ceria nanoparticles (50 or 20 nm size diameter, depending on the precipitating agent used) were synthetized by Wu et al. [33] with the reverse micelle systems and by Gawande and co-workers [35] with the wet impregnation protocol. Recently, in our research group, a simple and fast microwave-assisted hydrothermal procedure has been developed for the synthesis of magnetite nanoparticles, controlling both their morphology and growth [36]. Specifically, quasi-spherical (25 nm in size) and spheroidal (60 nm in size) Fe_3O_4 nanoparticles have been obtained by adding oleic acid and trisodium citrate to the reaction mixture, respectively; regular hexagonal magnetite nanoplatelets with a facet to-facet distance of 120 nm and a thickness of 53 nm and 40 nm have been recovered by using polyvinylpyrrolidone, as additive, or no additive, respectively. Following our studies on magnetite nanoparticles [36], we decided to add nanoceria to these Fe_3O_4 nanoparticles, to obtain Fe_3O_4/CeO_2 nanocomposites with different morphologies of magnetite seeds. The preparation method proposed in the present work is the microwave-assisted solvothermal synthesis in the presence of ethylene glycol. To the best of our knowledge this procedure has never been used before for the formation of Fe_3O_4/CeO_2 nanocomposites.

The aim of this study was to verify whether: (*i*) the nanoceria deposition process changes the pristine morphology of the magnetite nanoparticles, (*ii*) the different morphologies of magnetite seeds and the use of organic stabilizer (polyvinylpyrrolidone, trisodium citrate dihydrate or oleic acid) during preparation of the catalyst can influence its catalytic activity. The imine formation from benzyl alcohol and aniline was taken as the model reaction for catalytic tests.

Recently it has been reported that CeO_2 is the most active heterogeneous catalyst among various metal oxides tested (such as Al_2O_3, TiO_2, ZnO, etc.) for imine synthesis from alcohol and amine under air [37]. Furthermore, it has been proven that the efficiency of ceria for the synthesis of imine (whose importance stands in its role as intermediate for the preparation of various biological, agricultural and pharmaceutical compounds) is directly correlated with the number of oxygen vacancies onto the catalyst surface [38]. In particular, nanoceria prepared with the solvothermal method using ethylene glycol as the solvent has been found to have a number of oxygen vacancies higher than nanoceria synthetized with the hydrothermal procedure [38]. However, the poor recyclability of nanoceria, due to the difficulty of recovering caused by the highly powdery consistency of the nanomaterial, has limited its use as an efficient catalyst for imine formation. The use of the here presented Fe_3O_4/CeO_2 nanocomposites should overcome this problem, because the nano-catalysts are easily removable from the reaction mixture using an external magnet. In addition, the ceria nanoparticles deposited onto the magnetite seeds were prepared in our laboratory by avoiding the use of water as the solvent, i.e., under the best conditions for increasing the number of oxygen vacancies onto the ceria surface. All these features render the proposed synthesis procedure highly promising in the field of catalysis.

2. Results and Discussion

2.1. Synthesis of Magnetite/Ceria Nanocomposites

The deposition of ceria nanoparticles onto magnetite seeds was carried out by solvothermal method assisted by microwave irradiations, in order to overcome the common disadvantages proper of the classic solvothermal/hydrothermal procedure [39], i.e., difficult temperature control, slowness of the process, production of relatively large nanoparticles (mean diameter in the range 200–800 nm). The use of microwaves in the preparation of nanostructured materials has the advantage to increase the crystallinity of the nano powders and decrease the process times, and to favor homogeneous nucleation mechanisms leading to a narrow distribution of nanoparticle dimensions [40]. The magnetite seeds synthesis by microwave-assisted hydrothermal procedure led to morphologically different Fe_3O_4 nanoparticles, depending on the stabilizer used during their synthesis (polyvinylpyrrolidone (PVP), trisodium citrate dihydrate (CITR) and oleic acid (OA)) [36]. Their main features are reported in Table 1.

Table 1. Morphological features of Fe_3O_4 nanoparticles synthetized by microwave-assisted hydrothermal procedure [36] [a] Corresponding to the facet to facet distance.

Entry	Sample	Stabilizer	Shape	Mean Thickness [a] (nm)	Mean Diameter (nm)
1	Fe_3O_4	–	Hexagonal	40	120 [a]
2	Fe_3O_4:PVP	PVP	Hexagonal	53	116 [a]
3	Fe_3O_4:CITR	Trisodium citrate	Spheroidal	–	60
4	Fe_3O_4:OA	Oleic acid	*uasi*-Spheres	–	25

We decided to deposit nanoceria onto the nanoparticles reported in Table 1 by using the microwave-assisted solvothermal procedure (ethylene glycol as the solvent) to accelerate growth kinetics. All samples reported in Table 1 were subjected to ceria deposition, by using two different Ce/Fe_3O_4 molar ratios (0.6 and 1.5), followed by calcination under nitrogen (Scheme 1).

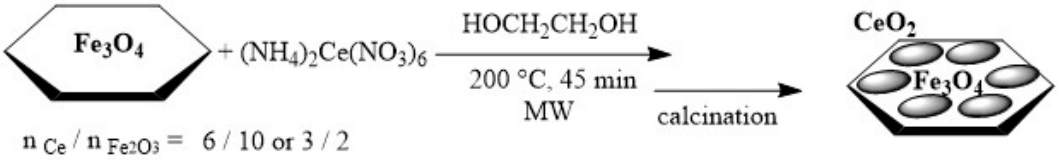

Scheme 1. Synthesis of Fe_3O_4/CeO_2 nanocomposites starting from hexagonal seeds of Fe_3O_4.

2.2. Thermogravimetric and Differential Scanning Calorimetry (TGA/DSC) Analyses

Figure 1 shows graphics obtained by thermogravimetric and differential scanning calorimetry (TGA/DSC) analyses of the nanocomposites (before calcination) obtained starting from the magnetite samples reported in Table 1, using a Ce/Fe_3O_4 molar ratio equal to 0.6 and 1.5, respectively.

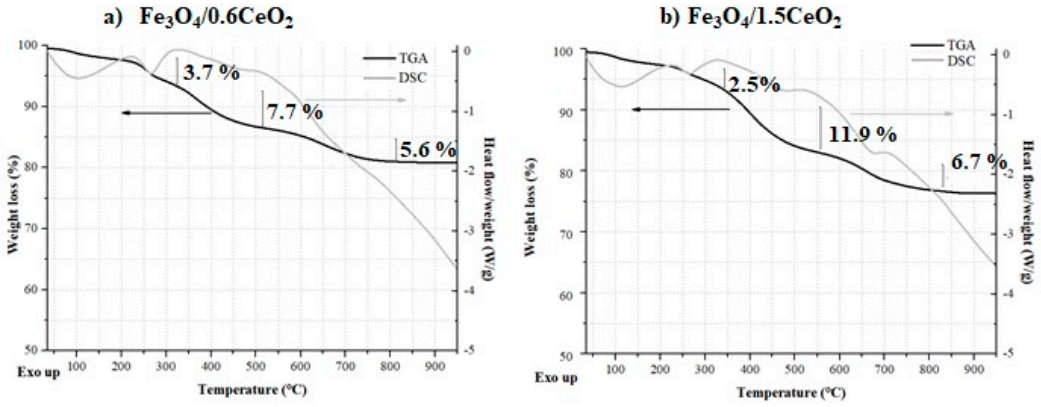

Figure 1. *Cont.*

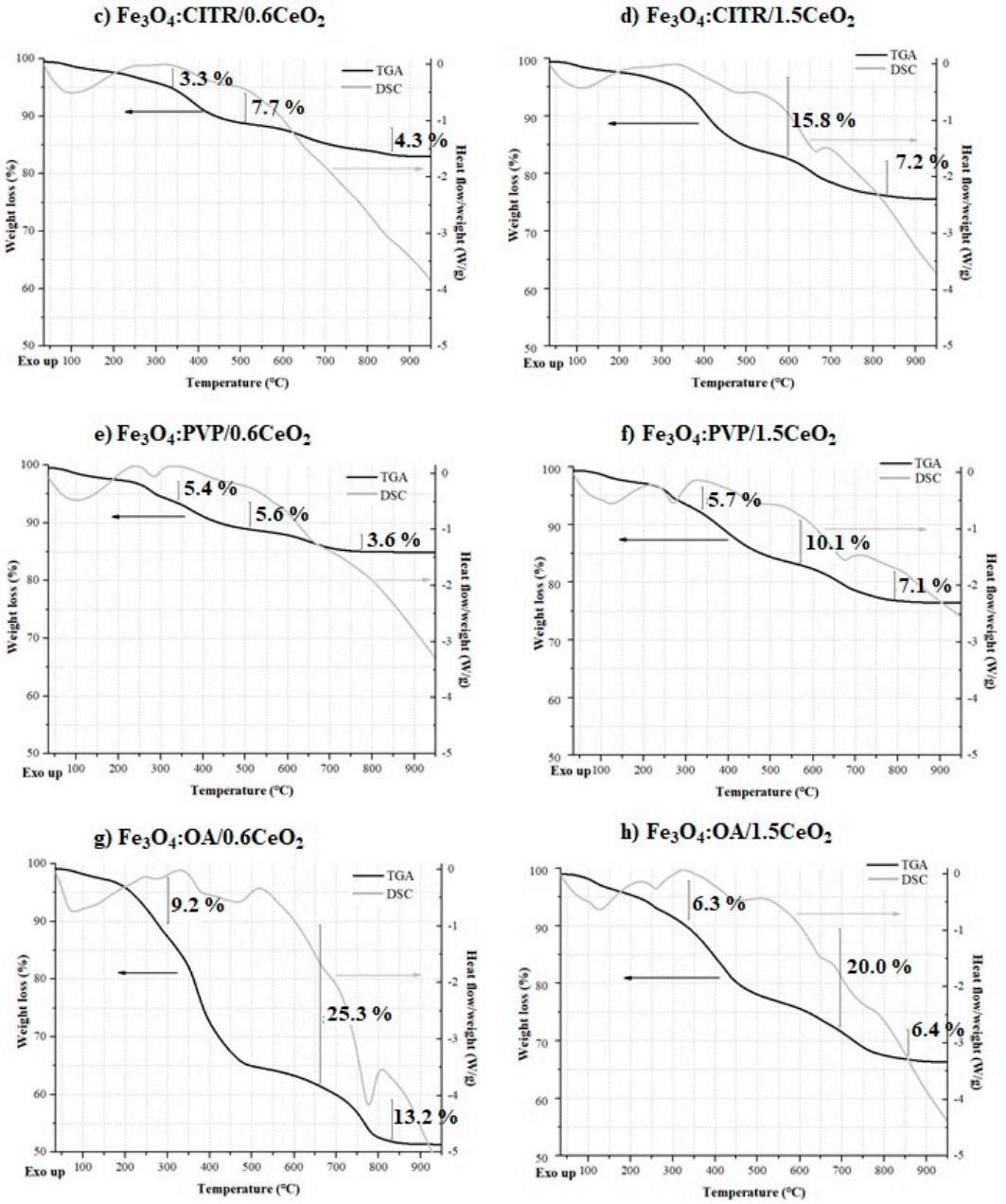

Figure 1. TGA (black) and DSC (grey) curves for: (**a**) Fe_3O_4/0.6CeO_2, (**b**) Fe_3O_4/1.5CeO_2, (**c**) Fe_3O_4:CITR/0.6CeO_2, (**d**) Fe_3O_4:CITR/1.5CeO_2, (**e**) Fe_3O_4:PVP/0.6CeO_2, (**f**) Fe_3O_4:PVP/1.5CeO_2, (**g**) Fe_3O_4:OA/0.6CeO_2 and (**h**) Fe_3O_4:OA/1.5CeO_2 samples.

TGA/DSC analyses revealed that, apart for the solvent mass loss, all samples underwent large weight loss in the temperature range 280–850 °C (13–26%) accompanied by endothermic processes [41], probably due to oxalate decomposition and leaching of organic ligands [38], that formed an inorganic–organic composite with ceria. Oxalate formation can be ascribable to the partial conversion of ethylene glycol to oxalic acid at high temperatures. Under the same reaction conditions, the cerium salt decomposed forming CeO_2, whose superficial hydroxy groups reacted with oxalic acid, giving rise to the above-mentioned polymeric inorganic-organic compound. Similar TGA behavior was observed by Yang and co-workers in nanoceria prepared by solvothermal synthesis in ethylene glycol [38]. However, DSC curves (Figure 1) show that all samples lose most of their weight around 500 °C due to CO and CO_2 emissions. Moreover, by increasing the temperature up to 1000 °C, a sintering peak in the DSC curve sometimes appears (see for example Figure 1g), indicative for sample melting, that compromises the

nature and therefore the functionality of the studied material. This phenomenon strongly suggests choosing a calcination temperature not higher than 550 °C. Finally, TGA/DSC curves of $0.6CeO_2$ and $1.5CeO_2$ (Figure S1) showed the same trend observed for all magnetite-ceria nanocomposites in the range 280–500 °C, due to oxalate decomposition and leaching of organic ligands. At temperatures higher than 550 °C the sintering processes are not observed due to the absence of magnetite.

2.3. IR Analyses

The observations revealed by TGA/DSC analyses were confirmed by IR studies. In fact, coordination of ethylene glycol and its decomposition products can be further proven by IR spectroscopy. Figure 2 shows IR spectra registered on all samples as prepared and recovered after TGA analysis, i.e., after calcination at 1000 °C under N_2 flow. IR spectra of all samples before calcination display a broad peak belonging to O–H stretching around 3417–3450 cm^{-1}, as well as a strong signal due to the asymmetric stretching of the O–C=O oxalate moiety in the range from 1632 cm^{-1} to 1602 cm^{-1}, and a sharp peak at ca. 1080 cm^{-1}, which corresponds to C–O vibrations, proving the coordination of the ethylene glycol to Ce through Ce–O–C bonds. Only spectra reported in Figure 2g,h before calcination show two characteristic peaks at 2918 and 2850 cm^{-1}, due to oleic acid C-H stretching. In addition, all IR spectra before calcination show both the Ce–O (470–490 cm^{-1}) stretching signals [42] and typical magnetite peaks, falling around 360, 450 and 580 cm^{-1} [43]. After calcination at 1000 °C, in all IR spectra, peaks due to organic moieties disappear and signals due to Fe_3O_4 structures modify, being shifted or vanishing, confirming what already found in TGA/DSC analyses, i.e., loss of the carbon ligands (at T > 550 °C) and modification of the Fe_3O_4/CeO_2 nanocomposite structure (at temperatures higher than 850 °C).

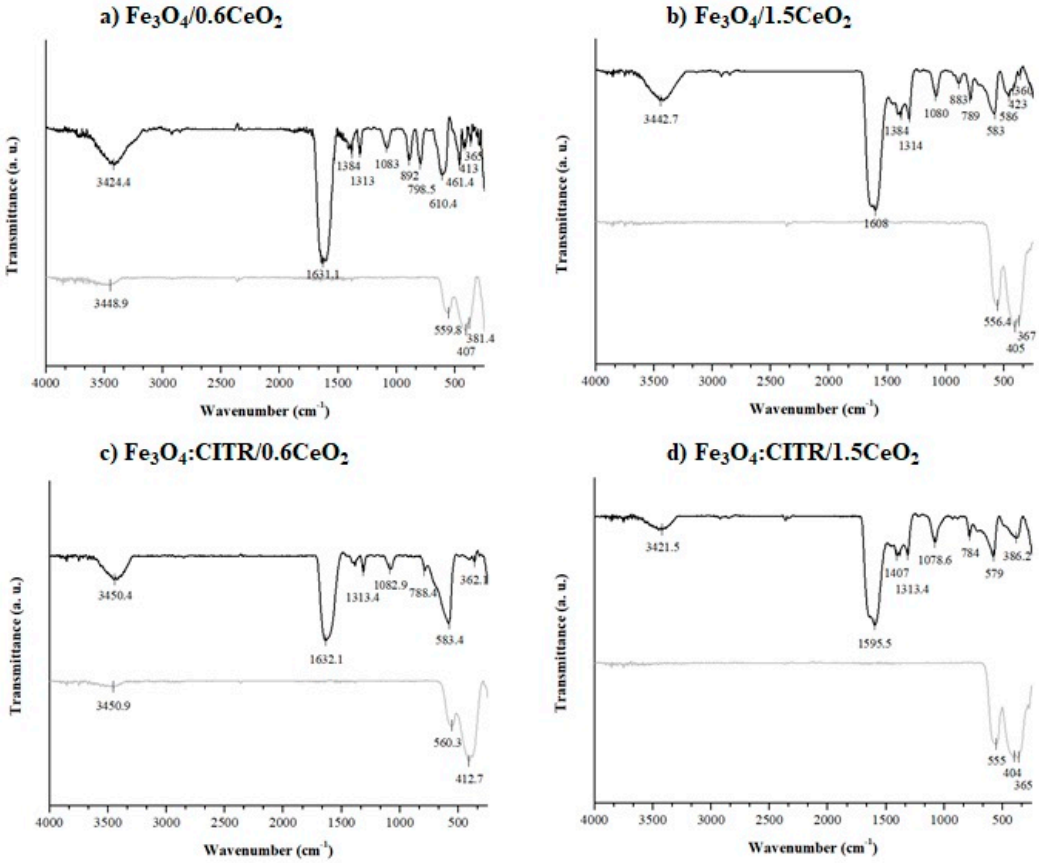

Figure 2. *Cont.*

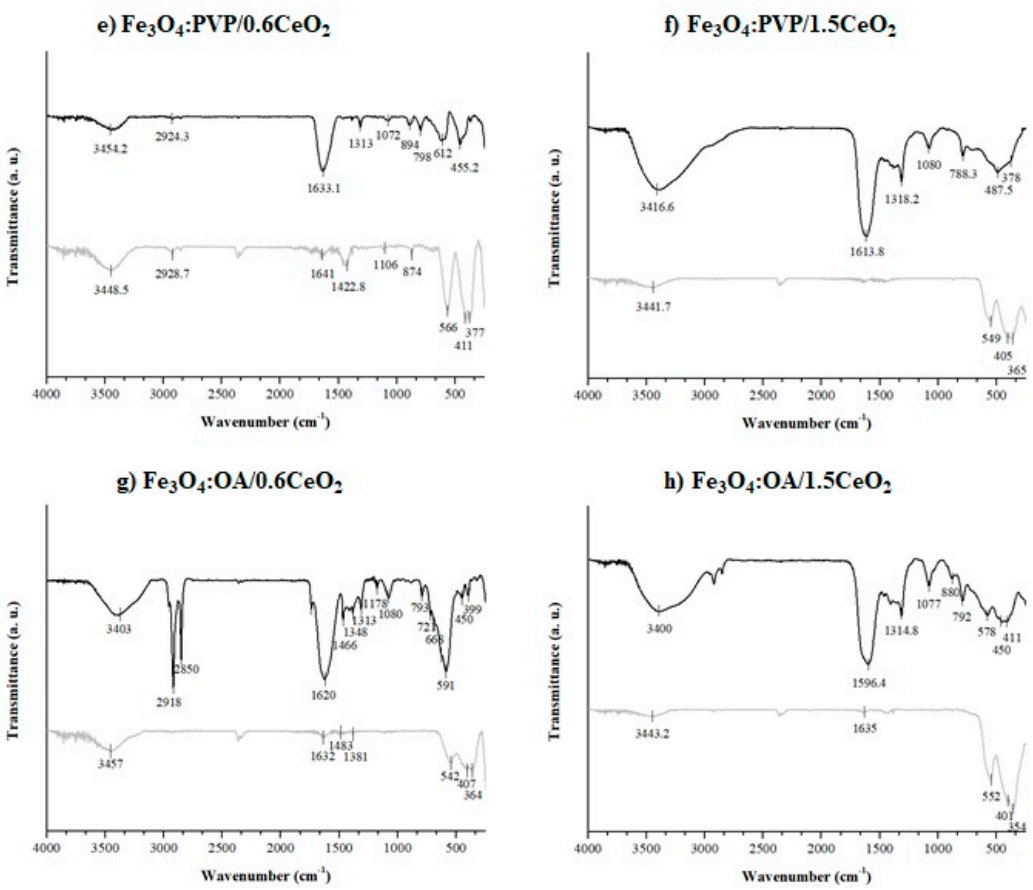

Figure 2. IR spectra of (**a**) Fe_3O_4/0.6CeO_2 (**b**) Fe_3O_4/1.5CeO_2, (**c**) Fe_3O_4:CITR/0.6CeO_2, (**d**) Fe_3O_4:CITR/1.5CeO_2, (**e**) Fe_3O_4:PVP/0.6CeO2, (**f**) Fe_3O_4:PVP/1.5CeO_2, (**g**) Fe_3O_4:OA/0.6CeO_2 and (**h**) Fe_3O_4:OA/1.5CeO_2, as prepared (black) and after calcination at 1000 °C (grey).

However, even after calcination at 1000 °C, all samples resulted magnetically active.

IR spectra of 0.6CeO_2 and 1.5CeO_2 (i.e., CeO_2 nanoparticles prepared under the same procedure of Fe_3O_4/0.6CeO_2 and Fe_3O_4/1.5CeO_2 respectively, but in the absence of magnetite), before and after calcination at 1000 °C, are reported in Figure S2 for comparison purposes. Before calcination, all peaks belonging to the formation of an organic-inorganic layer are evident. After calcination, the presence of only Ce–O stretching signals could be observed.

2.4. XRD Analyses

The as prepared and calcined (at 1000 °C) samples were also characterized by XRD. Aiming at recognizing the diffraction peaks belonging to neat CeO_2 prepared with the solvothermal method, the not-containing Fe_3O_4 seeds, i.e., 1.5CeO_2 and 0.6CeO_2 batches, were subjected to XRD analyses prior to all other nanocomposites. Figure 3 reports the diffraction peaks of 0.6CeO_2 and 1.5CeO_2 samples, before and after calcination at 1000 °C under nitrogen flow.

Figure 3 shows peaks at 28.0°, 32.7° and 47.0° 2θ corresponding to the (111), (200) and (220) crystal planes of ceria, respectively. They are sharp only in the XRD spectra of the calcined samples (Figure 3c,d), because the CeO_2 structure transition from the amorphous to the crystalline phase occurs at temperatures higher than 500 °C [42]. In addition, weak signals at 12.9 and 17.9° 2θ due to cerium (III) oxalate hydrate are present only before calcination (Figure 3a,b), suggesting that the organic cerium ligands, coming from the preparation step in ethylene glycol, decomposed at high temperatures.

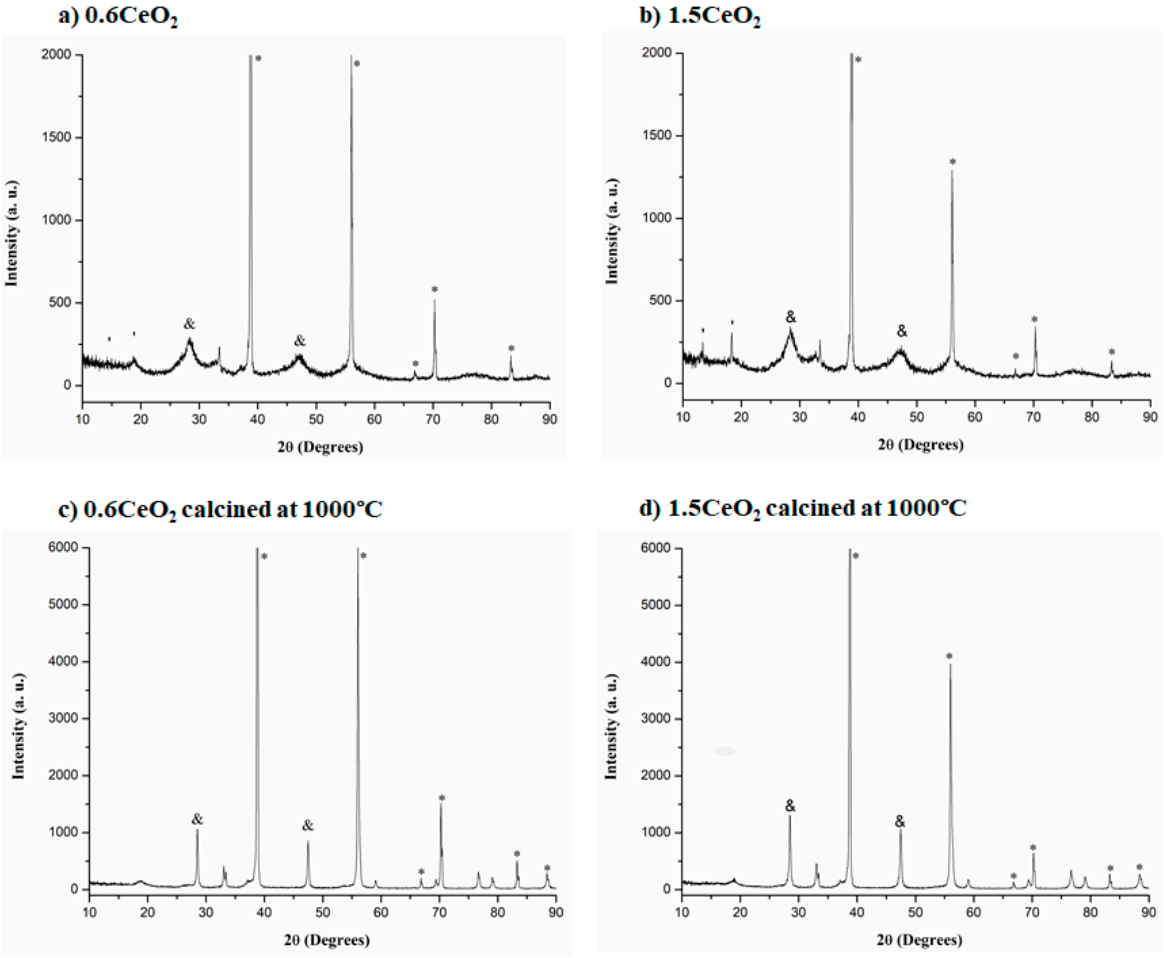

Figure 3. XRD patterns of (**a**) $0.6CeO_2$, (**b**) $1.5CeO_2$, (**c**) $0.6CeO_2$ and (**d**) $1.5CeO_2$ calcined at 1000 °C. The marked peaks belong to: * NaF (support), & ceria and ' cerium (III) oxalate hydrate.

Figure 4 reports the diffraction peaks of $Fe_3O_4/0.6CeO_2$ and $Fe_3O_4/1.5CeO_2$, before and after calcination at 1000 °C under nitrogen flow.

In the XRD spectra of $Fe_3O_4/0.6CeO_2$ (Figure 4a) and $Fe_3O_4/1.5CeO_2$ (Figure 4b), only the diffraction peaks belonging to magnetite are recognizable [36], and no ceria sharp signals are visible, as expected on the base of XRD spectra of $0.6CeO_2$ (Figure 3a) and $1.5CeO_2$ (Figure 3b) before calcination. After calcination at 1000 °C (Figure 4c,d), surprisingly no diffraction peak of crystalline ceria can be found. Instead of them, the spectra report the characteristics peaks of cerium ferrite, which formed during sintering processes occurring at temperatures higher than 600 °C. Moreover, in both calcined samples, wüstite (instead of magnetite) is detected with its characteristic peaks at 36.1°, 42.0° and 60.9° 2θ, belonging respectively to the (111), (200) and (220) planes (Figure 4c,d). Weak peaks of magnetite are detected only in the calcined $Fe_3O_4/0.6CeO_2$ composite (Figure 4c).

Figures 5 and 6 show XRD spectra of all eight nanocomposites calcined at 1000 °C. Notably, signals belonging to wüstite and cerium ferrite can be observed in all of them.

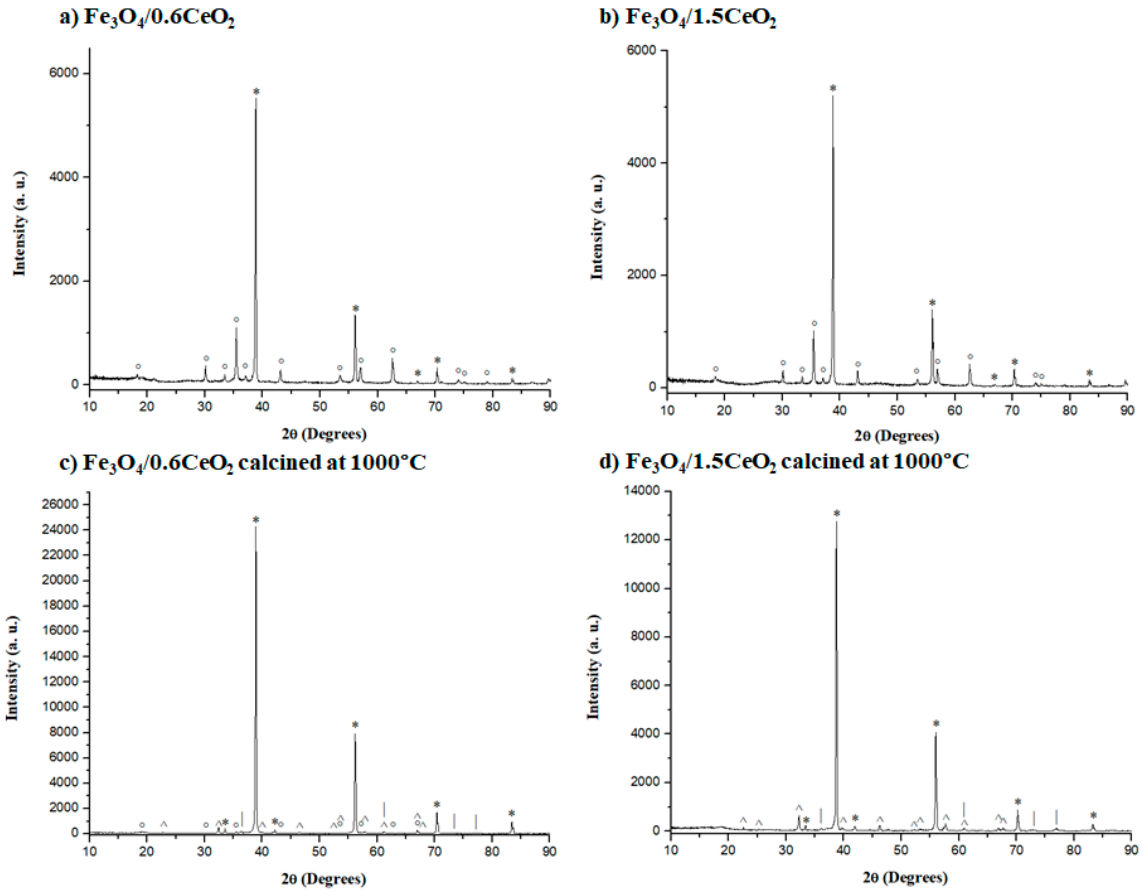

Figure 4. XRD patterns of (**a**) $Fe_3O_4/0.6CeO_2$, (**b**) Fe_3O_4/ $1.5CeO_2$, (**c**) $Fe_3O_4/0.6CeO_2$ and (**d**) Fe_3O_4/ $1.5CeO_2$ calcined at 1000 °C. The marked peaks belong to: * NaF (support), ° magnetite, ˆ cerium ferrite and | wüstite.

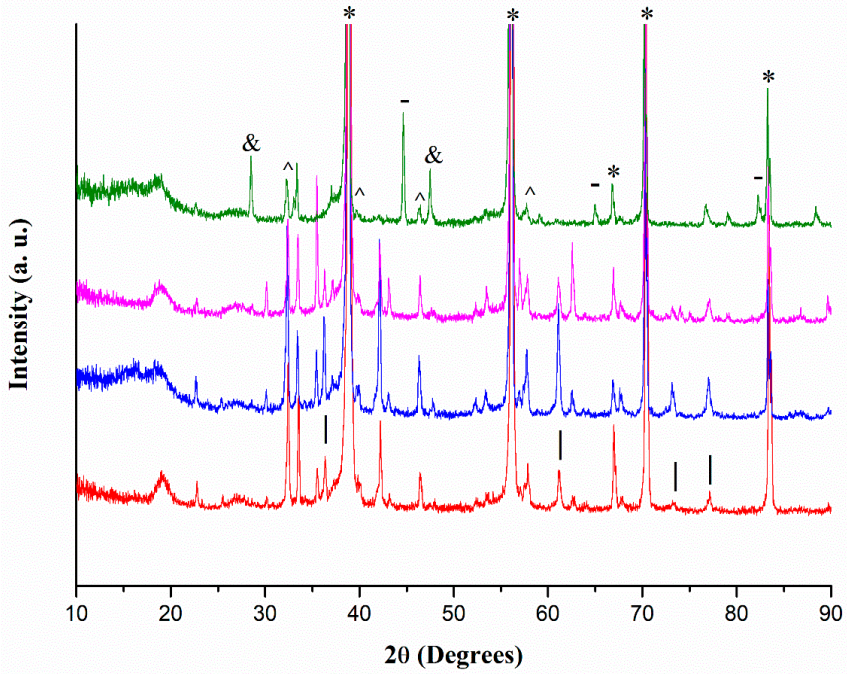

Figure 5. XRD patterns of samples calcined at 1000 °C of: $Fe_3O_4/0.6CeO_2$ (red line); F_3O_4:CITR/$0.6CeO_2$ (blue line); Fe_3O_4:PVP/$0.6CeO_2$ (magenta line); Fe_3O_4:OA/$0.6CeO_2$ (green line). The marked peaks belong to: * NaF (support); & ceria; ˆ cerium ferrite; - Fe; | wüstite.

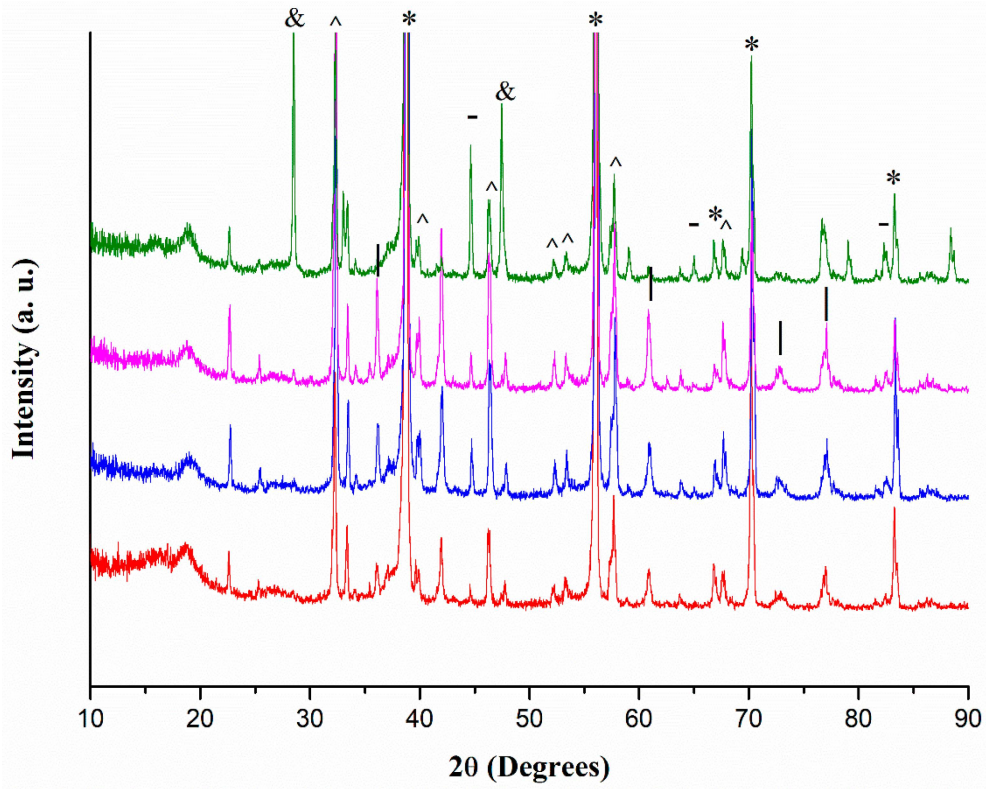

Figure 6. XRD patterns of samples calcined at 1000 °C: Fe_3O_4/1.5CeO_2 (red line); F_3O_4:CITR/1.5CeO_2 (blue line); Fe_3O_4:PVP/1.5CeO_2 (magenta line); Fe_3O_4:OA/1.5CeO_2 (green line). The marked peaks belong to: * NaF (support); & ceria; ^ cerium ferrite; - Fe; | wüstite.

2.5. TEM Analyses

TEM images of Fe_3O_4/0.6CeO_2 (Figure 7a) and Fe_3O_4/1.5CeO_2 (Figure 7b) revealed that the original hexagonal morphology of the magnetite seeds was retained. However, a close inspection of the TEM image of Fe_3O_4/0.6CeO_2 (Figure 7a) highlighted that hexagonal magnetite seeds were not sticked to nanoceria. On the contrary, in the case of Fe_3O_4/1.5CeO_2 (Figure 7b) nanoceria was adherent to Fe_3O_4 nanoparticles. This evidence suggested us to consider, for possible catalytic purposes only, nanocomposites obtained by using a Ce/Fe_3O_4 molar ratio equal to 1.5.

TEM images of calcined (at 1000 °C) Fe_3O_4/0.6CeO_2 (Figure S3a) and Fe_3O_4/1.5CeO_2 (Figure S3b) confirmed what found with other analyses, i.e., the sintering of cerium and iron compounds at nanoscale levels. The occurrence of melting processes at high temperatures were also revealed by FESEM image of Fe_3O_4/1.5CeO_2 calcined at 1000 °C (Figure 7c), where the hexagonal nanoparticles of magnetite are not visible anymore.

2.6. Calcination at 550 °C

All the discussed analyses revealed the occurrence of sintering processes in all nanocomposites calcined at 1000 °C. Moreover, TGA/DSC experiments showed that this degradation starts at temperature higher than 600 °C. In addition, TEM images evidenced the poorness of the amount of ceria in nanocomposites prepared by using a Ce/Fe_3O_4 molar ratio equal to 0.6. For these reasons, only samples synthetized with a Ce/Fe_3O_4 molar ratio equal to 1.5 were considered for further studies (including catalytic tests), and a new calcination temperature was chosen. It was set at 550 °C, as the best value, because it is lower than 600 °C in order to avoid sintering progressions, but high enough to allow the transition of ceria from the amorphous to the crystalline phase [44].

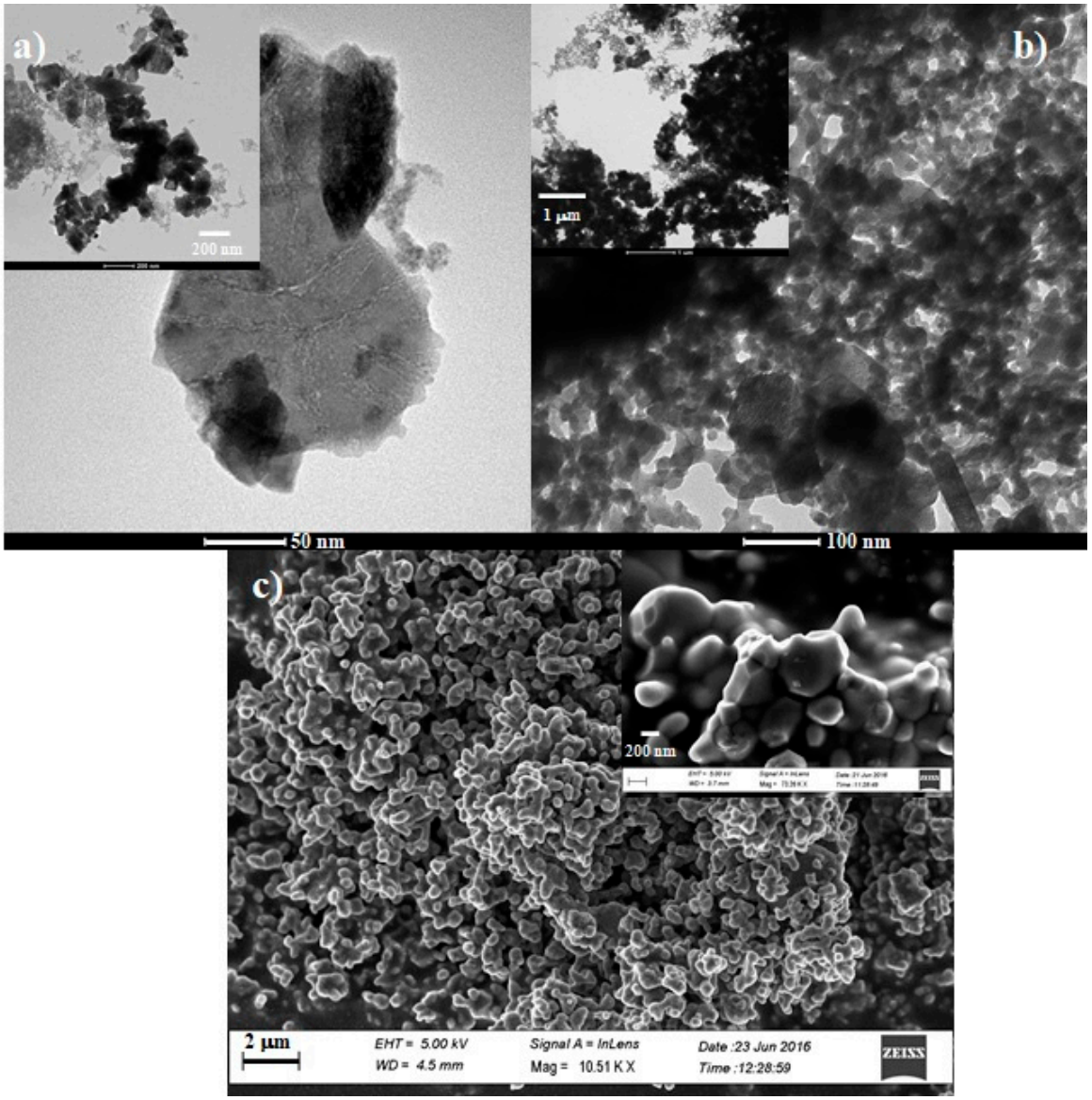

Figure 7. TEM images of (**a**) $Fe_3O_4/0.6CeO_2$, (**b**) $Fe_3O_4/1.5CeO_2$. (**c**) FESEM image of $Fe_3O_4/1.5CeO_2$ calcined at 1000 °C.

Thus, all nanocomposites synthetized with 1.5 Ce/Fe_3O_4 molar ratio were calcined at 550 °C and subjected to XRD, IR, FESEM and EDS analyses.

Their XRD spectra (Figure 8) show diffraction peaks belonging to both ceria and magnetite, besides the absence of signals due to sintering compound (cerium ferrite). Notably, the particle sizes of crystalline CeO_2 calculated by the Scherrer formula (Figure 8) range between 4.1 and 4.9 nm, highlighting their nanoscopic dimension. On the contrary, the particle size of the same samples calcined at 1000 °C ranges from 37.7 to 56.7 nm, due to the occurrence of sintering processes.

A perusal of XRD patterns led us to the following observations on the nanocomposites prepared with the addition of OA (green lines of Figures 5, 6 and 8): (*i*) XRD patterns of OA samples after calcination at 1000 °C (Figures 5 and 6) show the presence of crystalline CeO_2, whereas other samples do not; (*ii*) OA samples show the presence of Fe-metal (particularly in Figure 5); (*iii*) after calcination at 550 °C, the OA sample shows much less magnetite (Figure 8). All these occurrences, together with the observation that the weight loss, as determined by TGA (Figure 1) being much higher for both OA samples (Figure 1g,h), are indicative for the presence of much more organic compounds with respect to the other prepared nanocomposites. From these observations, it can be concluded that a higher amount

of pyrolysis products from oleic acid and/or ethylene glycol is present in OA samples. This seems to have a significant influence on phase formation. An effect on the 'melting' in TGA curve of sample g) (Figure 1) could also be possible and partial carbothermal reduction of iron oxide to metal iron can be promoted. In fact, thermodynamically, the reduction of iron oxide occurs in steps. Accordingly, the following stable iron oxides can form during the reduction (above 570 °C): hematite, magnetite and non-stoichiometric wüstite. During the stepwise reduction of magnetite to wüstite, metallic iron is generally produced [45]. TGA/DSC analyses of magnetite/ceria nanocomposites (Figure 1) revealed the occurrence of a carbothermal reduction of magnetite: wüstite was first formed followed by metallic iron. Direct reduction of iron oxides by solid carbon has also been reported and the carbon source could be coke, graphite, coal, char, deposited carbon and activated carbon [46]. The presence of carbon can change the activation and the rate of the reduction of magnetite to wüstite and metallic iron. In fact, by TGA/DSC analyses of Fe_3O_4:OA/0.6CeO_2 and Fe_3O_4:OA/1.5CeO_2 (Figure 1g,h), a high content of organic ligands were detected due to higher weight loss in the temperature range between 350 °C and 450 °C with respect to the other magnetite/ceria nanocomposites. The presence of a high content of carbon in the Fe_3O_4:OA/0.6CeO_2 and Fe_3O_4:OA/1.5CeO_2 samples led to a more pronounced endothermic peak at ca. 750 °C ascribable to the carbothermal reduction [45].

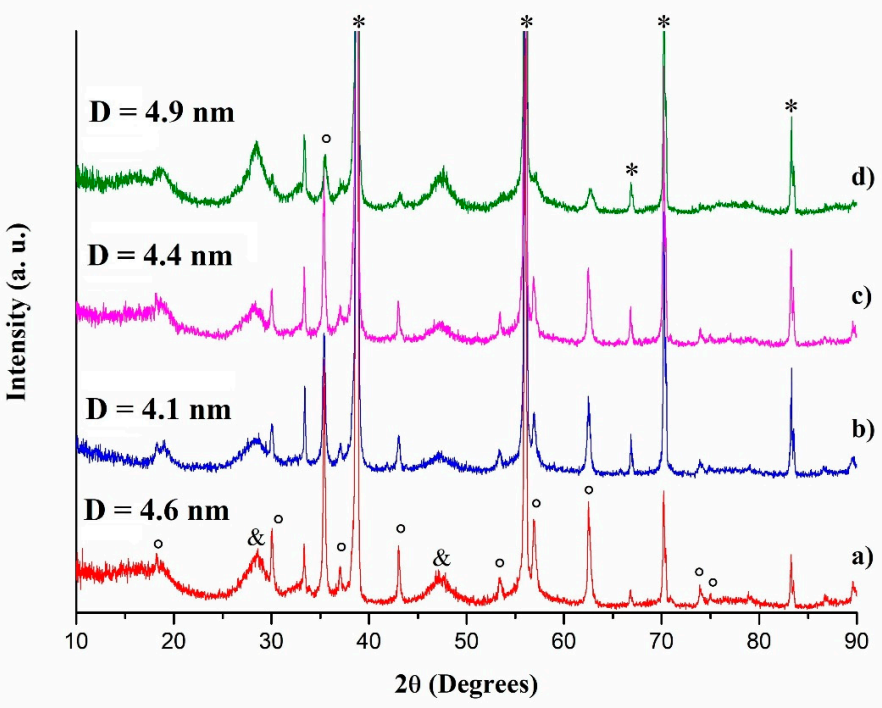

Figure 8. XRD patterns of samples calcined at 550 °C: (**a**) Fe_3O_4/1.5CeO_2 (red line); (**b**) Fe_3O_4:CITR/1.5CeO_2 (blue line); (**c**) Fe_3O_4:PVP/1.5CeO_2 (magenta line); (**d**) Fe_3O_4:OA/1.5CeO_2 (green line). The marked peaks belong to: * NaF (support); ° magnetite; & ceria. **D** is the particle size of crystalline ceria, calculated by the Scherrer formula based on the strongest peak (111) of CeO_2 at ca. 2θ = 28.5°.

All nanocomposites calcined at 550 °C were analyzed by IR spectroscopy. IR spectra (Figure 9) display typical peaks of ceria and magnetite in the range of 360–580 cm^{-1} and the absence of signal ascribable to any organic ligands (over the detection limit of the analytical technique), proving the loss of the majority of the organic layer and the presence of both CeO_2 and Fe_3O_4 in the nanocomposites.

Finally, all samples calcined at 550 °C were investigated by FESEM spectroscopy. FESEM micrographs (Figure 10) show that the pristine morphology of magnetite nanoparticles was kept after ceria deposition. In fact, in both Fe_3O_4/1.5CeO_2 and Fe_3O_4:PVP/1.5CeO_2 (Figure 10a,c) the hexagonal structure observed in Fe_3O_4 and Fe_3O_4:PVP seeds was maintained [36], while Fe_3O_4:CITR/1.5CeO_2 and Fe_3O_4:OA/1.5CeO_2 (Figure 10b,d) showed an almost or completely spherical structure, as well as their respective precursors [36].

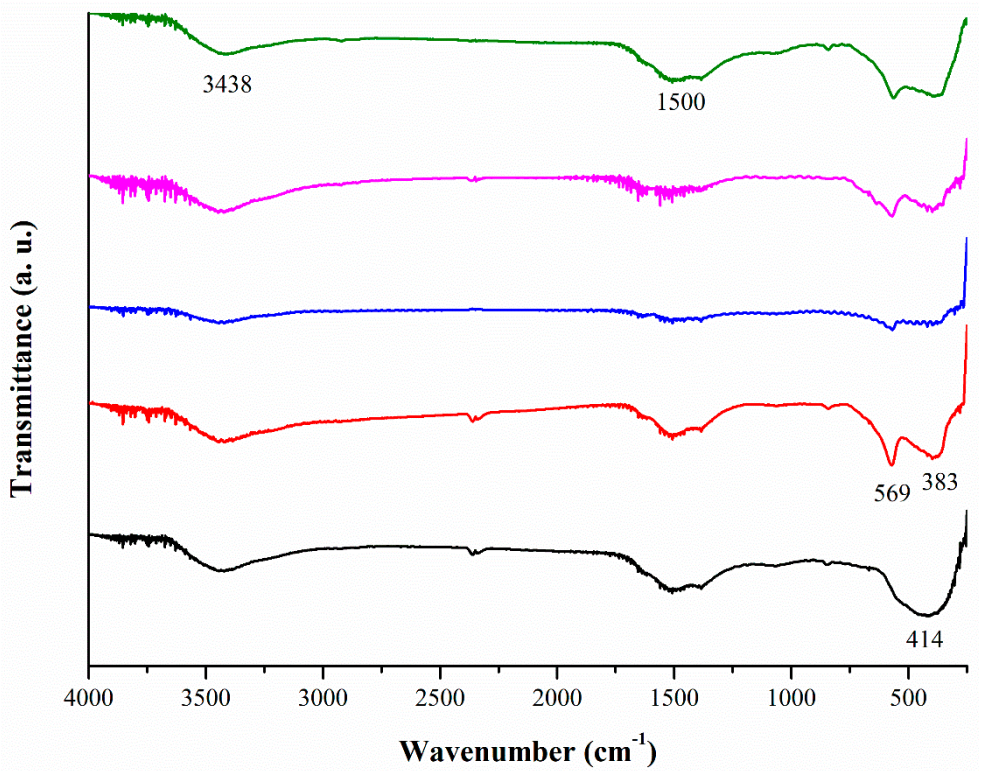

Figure 9. IR spectra (KBr) of samples calcined at 550 °C: Fe_3O_4/1.5CeO_2 (green line); Figure 3 red line); Fe_3O_4:PVP/1.5CeO_2 (blue line); Fe_3O_4:OA/1.5CeO_2 (magenta line); 1.5CeO_2 (black line).

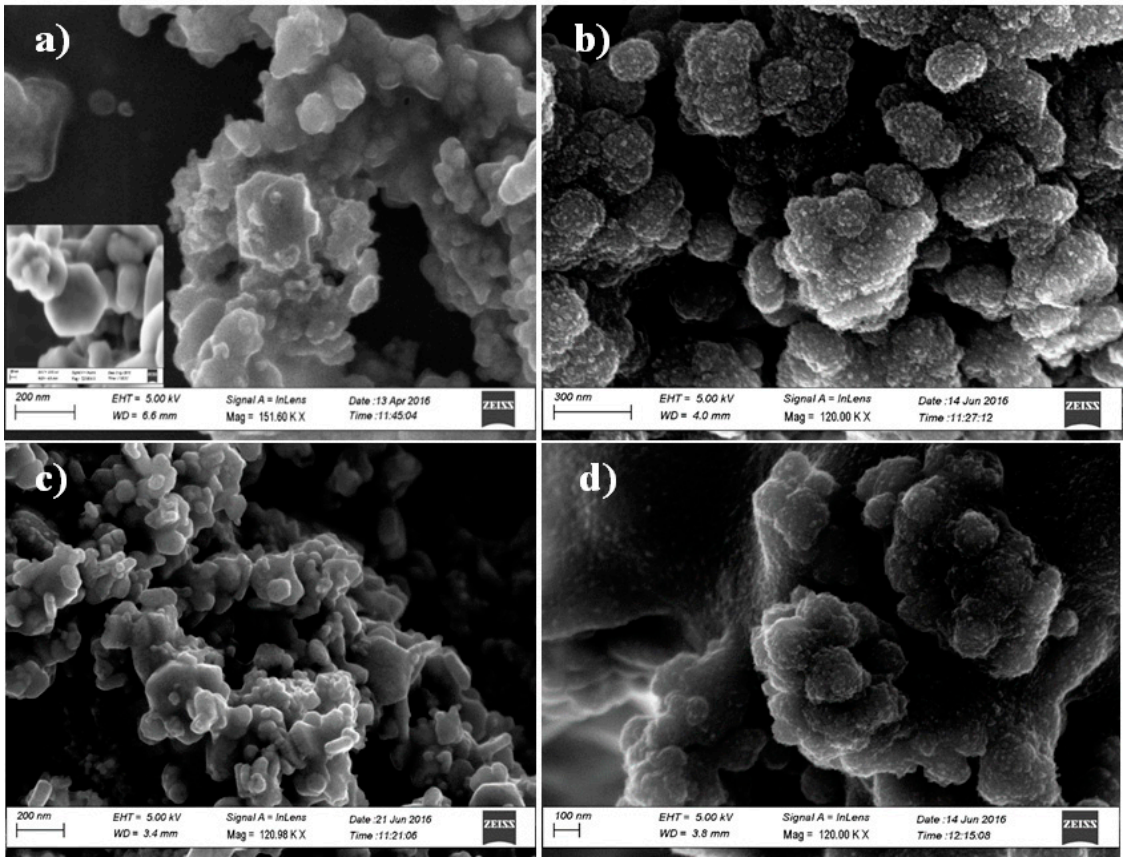

Figure 10. FESEM images of samples calcined at 550 °C: (**a**) Fe_3O_4/1.5CeO_2; (**b**) Fe_3O_4:CITR/1.5CeO_2; (**c**) Fe_3O_4:PVP/1.5CeO_2; (**d**) Fe_3O_4:OA/1.5CeO_2.

In addition, the presence of ceria nanoparticles was confirmed by EDS analyses (Figures S4–S7), but the core-shell structure was not observed. All materials were magnetite/ceria nanocomposites, in which the pristine morphologies of Fe_3O_4 seeds were retained after CeO_2 deposition. EDS elemental analyses revealed the following CeO_2/Fe_3O_4 mass ratio in the nanomaterials calcined at 550 °C: 14/86, 18/82, 21/79, 13/87 in Fe_3O_4/1.5CeO_2, Fe_3O_4:CITR/1.5CeO_2 Fe_3O_4:PVP/1.5CeO_2 and Fe_3O_4:OA/1.5CeO_2, respectively. Furthermore, EDS spectra (Figures S4–S7) also showed the presence of C and O, as well as the absence of N in all samples. The presence of C residual species would affect the catalytic activity of the nanocomposites (see the next paragraph).

The calcination temperature also affected the porosity of the nanocomposites, as highlighted by Figure 11, reporting the change of morphology of Fe_3O_4/1.5CeO_2 by passing from the pristine state to the forms after calcination at 550 °C and 1000 °C, respectively. The mesoporous structure observed after calcination at 550 °C should be useful for catalytic purposes, as it facilitates the arrival of substrates and/or intermediates to the catalytically active sites.

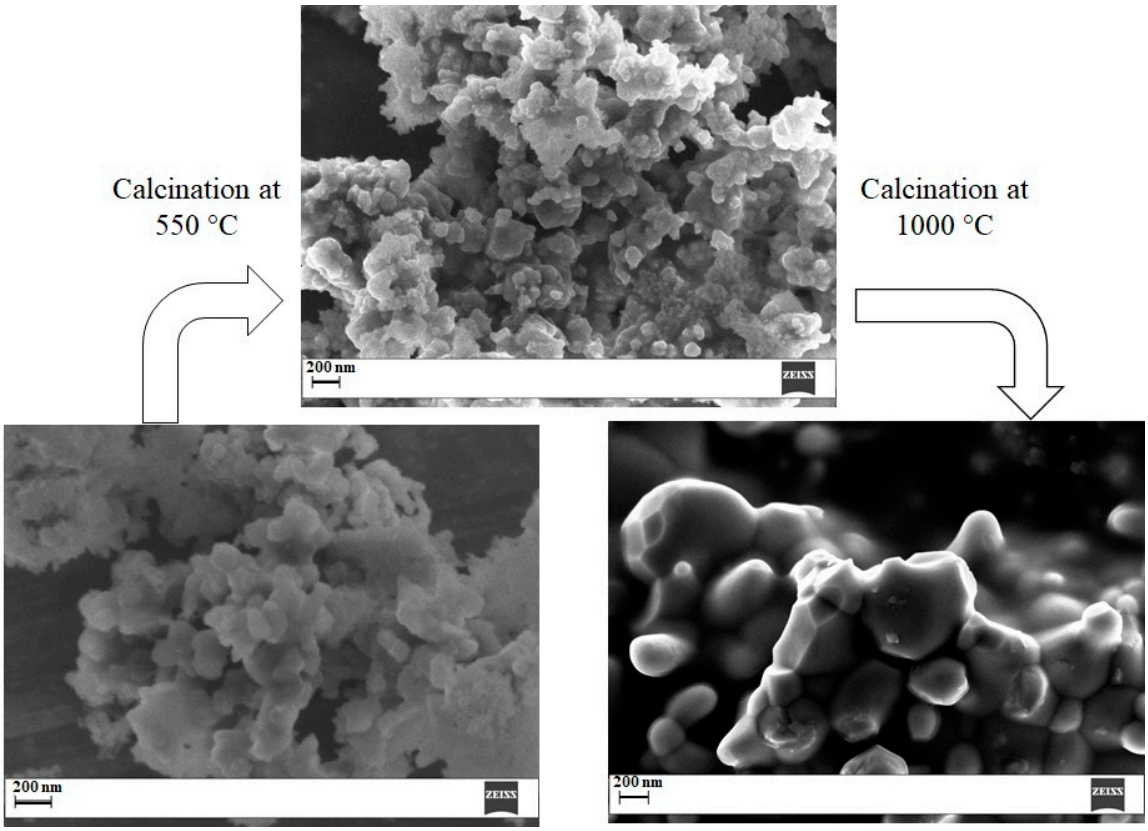

Figure 11. Change of morphology of Fe_3O_4/1.5CeO_2 at different calcination temperatures.

2.7. Catalytic Tests

All nanocomposites synthetized with a Ce/Fe_3O_4 molar ratio equal to 1.5 and calcined at 550 °C were tested as catalysts in the aerobic imine formation reaction, starting from aniline and benzyl alcohol under solvent less conditions (Scheme 2). The catalytic test was designed on the base of Tamura [37] experiments by using benzyl alcohol (0.2 mmol) and aniline (0.4 mmol) in the presence of 10 mg CeO_2 without solvent at 323 K. As suggested by Yang [38], the reaction rates were employed for assessing the catalytic ability, calculating the imine formation amount per hour per ceria amount (mmol $h^{-1}g^{-1}$).

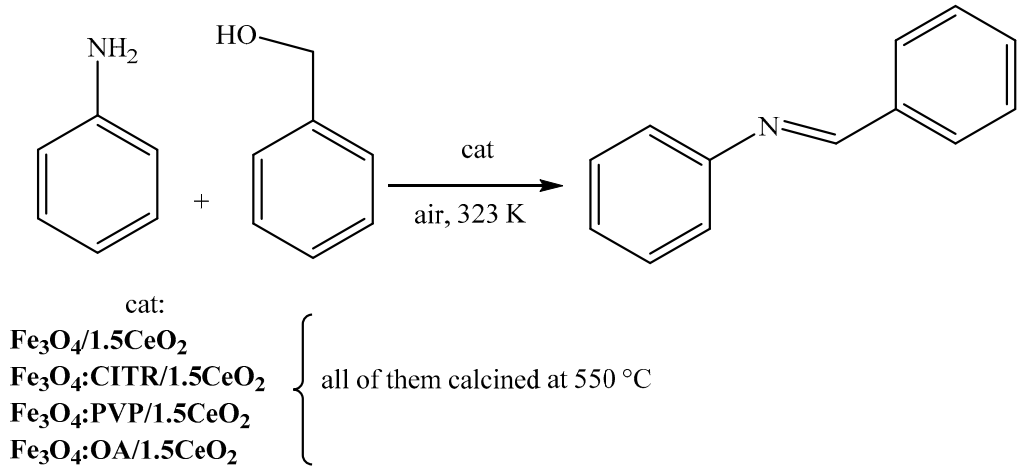

Scheme 2. Imine synthesis from benzyl alcohol and aniline over various nanocomposites.

Figure 12 shows the catalytic activity of the various nanocomposites employed for the imine formation reaction under the conditions reported in Scheme 1. Negligible conversion of the substrate was observed in the absence of any catalyst, while a good rate of 1.34 mmol $h^{-1}g^{-1}$, comparable to the value reported by Yang [38], was obtained in the presence of $Fe_3O_4/1.5CeO_2$. Unsatisfactory imine formation rate values of 0.16 mmol $h^{-1}g^{-1}$, 0.58 mmol $h^{-1}g^{-1}$ and 0.63 mmol $h^{-1}g^{-1}$ were observed for Fe_3O_4:CITR/$1.5CeO_2$, Fe_3O_4:PVP/$1.5CeO_2$ and Fe_3O_4:OA/$1.5CeO_2$, respectively. This means that the reaction rate for imine synthesis from benzyl alcohol and aniline over various nanocomposites was the best in the case of the catalyst obtained without any organic stabilizers. It can suggest that the part of catalytically active centers might be blocked by coke deposited on the surface of catalysts.

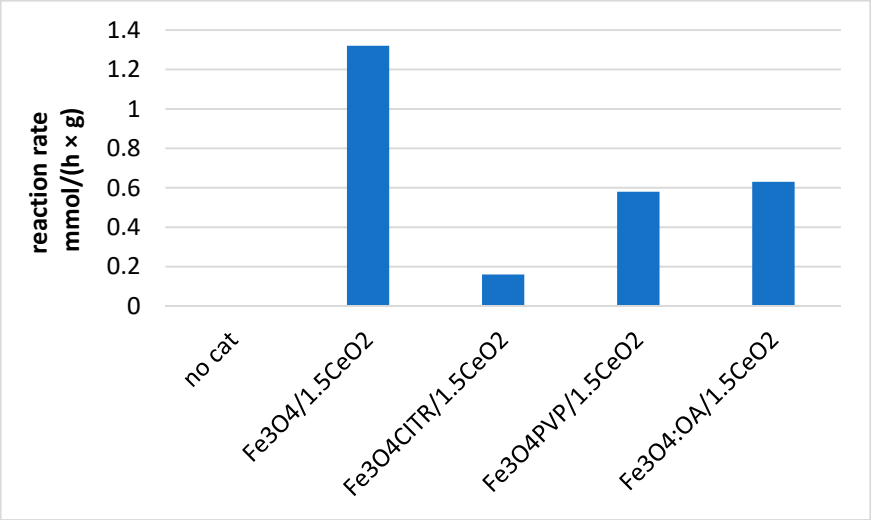

Figure 12. Catalytic activity of various nanocomposites for the imine formation reaction under the conditions reported in Scheme 2.

The recyclability tests were carried out only with the most active catalyst, i.e., $Fe_3O_4/1.5CeO_2$. Thus, at the end of the reaction, $Fe_3O_4/1.5CeO_2$ was removed from the reaction mixture by the use of an external magnet, then it was washed with ethanol and calcined under air at 400 °C for 3 h, before being used for a subsequent run. This calcination process was necessary to clear the oxygen vacancies (i.e., the catalytically active sites) possibly occupied by water oxygen [47], since water was contained in the ethanol solvent used during the recovery work-up of the catalyst. In fact, in the absence of the calcination step before reuse, the catalytic activity of the nanocomposite dramatically dropped to 0.39 mmol $h^{-1}g^{-1}$ for the presence of hydroxylic groups on the ceria surfaces. Figure 13

reports the recyclability of $Fe_3O_4/1.5CeO_2$ calcined under air at 400 °C for 3 h before each subsequent catalytic cycle. The activity of the catalyst increased with the reuses reaching imine formation rate of 2.3 mmol $h^{-1}g^{-1}$ and the catalyst resulted magnetically active after each run. For comparison purposes, the catalytic activity of commercial nanoceria, calcined at 400 °C for 3 h under air before use, was studied. The observed reaction rate was 0.34 mmol $h^{-1}g^{-1}$ (Figure 13), even lower than the value reached with $Fe_3O_4/1.5CeO_2$ in the first run, proving that the catalyst morphology strongly affects its catalytic activity.

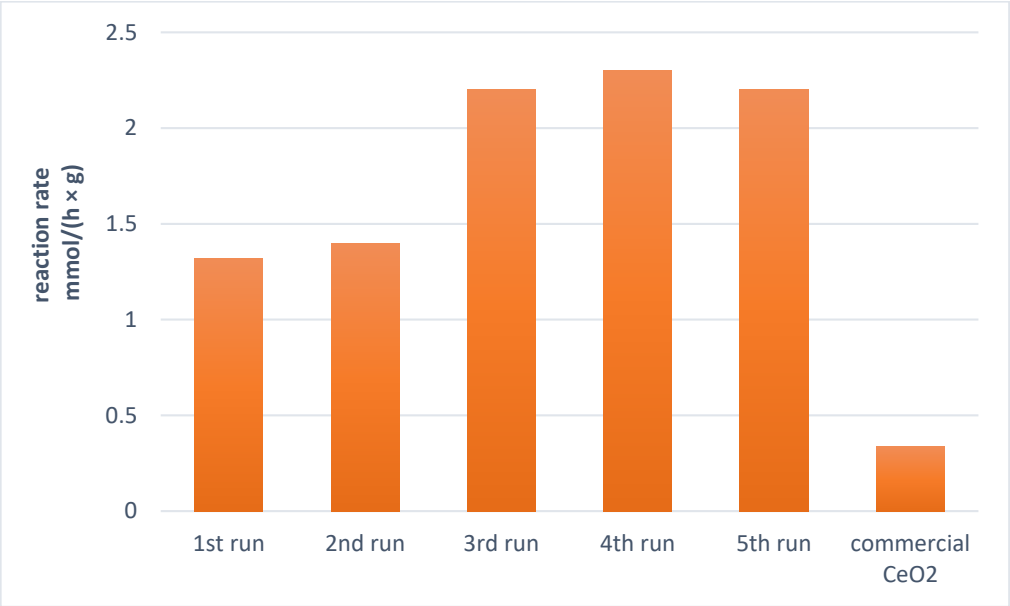

Figure 13. Recyclability of $Fe_3O_4/1.5CeO_2$ in the imine formation reaction, under the reaction conditions reported in Scheme 1. The last histogram is referred to commercial nanoceria calcined at 400 °C for 3 h under air.

In addition, $Fe_3O_4/1.5CeO_2$ nanocomposite was more active than other commercial metal oxides for catalyzing the considered model reaction (Table S2).

To get insight into the structure changes of the nanocomposite with the recycles, $Fe_3O_4/1.5CeO_2$ recovered after five subsequent runs was subjected to XRD analyses. The diffraction pattern of the used catalyst (Figure 14) resembles the one reported in the XRD spectrum of the same nanocomposite before its use in catalysis (Figure 8a), showing the typical peaks belonging to ceria and magnetite. Both XRD spectra (Figures 8a and 14) display a very broad signal below 17.9°, which can contain diffraction peaks of magnetite, cerium (III) oxalate hydrate and even iron (II) oxalate dihydrate (humboltite). In the XRD spectrum of the recovered catalyst (Figure 14), ceria peaks are more intense than the broad signal below 17.9°, while in the spectrum of the pristine catalyst their intensities are similar, thus explaining the increasing of the catalytic activity with the reuses, probably due to degradation of the organic impurities (oxalates) coming from the solvothermal synthesis. In fact, all organic ligands (oxalate, ethylene glycol derivatives, etc.) formed during the preparation of the catalyst, can occlude the catalytically active sites. Their removal might benefit the activity of the whole catalyst.

The plausible mechanism [37] commonly accepted for the imine synthesis over ceria is reported in Scheme 3 and it is based on the redox properties of ceria, because the oxidative dehydrogenation of benzyl alcohol occurs when cerium is reduced from +4 to +3 oxidation state. Afterwards, benzaldehyde reacts with aniline to afford imine, and cerium is in turn oxidized from +3 to +4 oxidation state by dioxygen to start a new cycle. In addition, Zhang et al. [38] have already demonstrated that the catalytic activity of CeO_2 in the oxidative imine formation reaction is related to oxygen vacancies and Ce^{3+} amount in the surface of the catalyst.

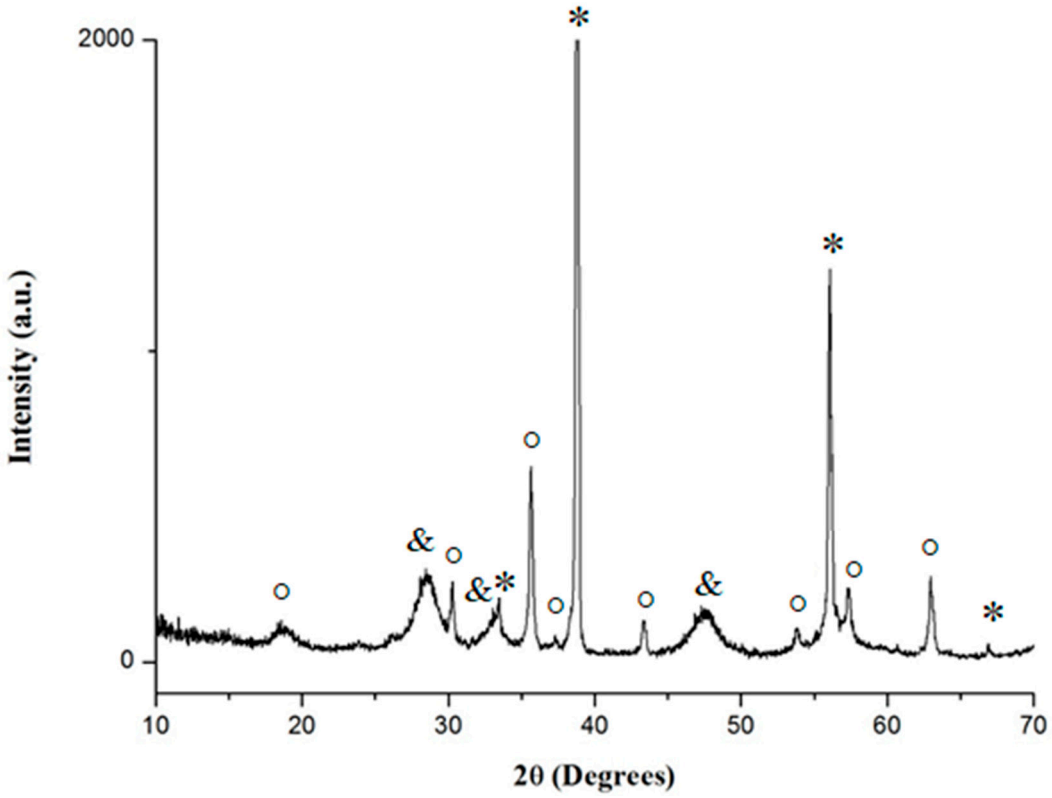

Figure 14. XRD patterns of $Fe_3O_4/1.5CeO_2$ recovered after five subsequent catalytic runs. The marked peaks belong to: * NaF (support); ° magnetite; & ceria.

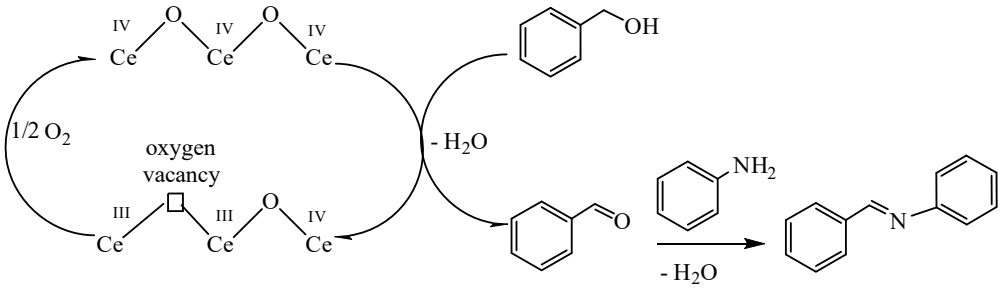

Scheme 3. Proposed mechanism for the imine synthesis over ceria.

FT-IR spectrum of $Fe_3O_4/1.5CeO_2$ after calcination for 3 h at 400 °C (Figure S8) displays typical peaks of ceria and magnetite in the range of 360–580 cm^{-1}. O–H stretching broad signal are still visible because calcination and subsequent cooling were carried out under air. Although it has been demonstrated that calcination under inert atmosphere leads to a higher number of oxygen vacancies over ceria surface than calcination under air [2], in the case of $Fe_3O_4/1.5CeO_2$, air is necessary during calcination, because it burns coke residues that may occlude catalytically active sites.

3. Experimental

3.1. Materials and Methods

Tap water was de-ionized by ionic exchange resins (Millipore, Darmstadt, Germany) before use. Commercial ferrous chloride tetrahydrate (99.9%,VWR, Milan, Italy), ceric ammonium nitrate (98.5%, VWR, Milan, Italy), ceria nanoparticles CeO_2 (<25 nm, Sigma-Aldrich, Milan, Italy), sodium hydroxide pearls (99.0%, Carlo Erba, Milan, Italy), hydrazine monohydrate (98.0%, Sigma-Aldrich, Milan, Italy) 64–65% (*v*/*v*) aqueous solution, oleic acid (OA, 90%, Alfa-Aesar, Kandel, Germany), trisodium citrate

dihydrate (CITR, 99%, Sigma-Aldrich, Milan, Italy), polyvinylpyrrolidone (PVP, MW = 40,000 Da, Sigma-Aldrich, Milan, Italy) and absolute ethanol (99.5%, Sigma-Aldrich, Milan, Italy) were used as received.

Microwave-assisted solvothermal syntheses were carried out in an ETHOS E-TOUCH Milestone (Sorisole (BG), Italy) applicator, using the conditions described in the following Section 3.2.

Catalytic reactions were monitored by GLC or by gas chromatography-mass spectroscopy (GC-MS) analyses. GLC analyses were performed using a HP 6890 instrument equipped with FID detector and a HP-1 (Crosslinked Methyl Siloxane) capillary column (60.0 m × 0.25 mm × 1.0 μm). Conversions and yields were calculated by GLC analysis using biphenyl as the internal standard. GC-MS data (EI, 70 eV) were acquired on a HP 6890 instrument (HP-Agilent, Santa Clara, CA, USA) using a HP-5MS cross-linked 5% PH ME siloxane (30.0 m × 0.25 mm × 0.25 μm) capillary column coupled with a mass spectrometer HP 5973 (HP-Agilent, Santa Clara, CA, USA). The products were identified by comparison of their GC-MS features with those of authentic samples.

FT-IR spectra (in KBr pellets) were recorded on a Jasco FT/IR 4200 spectrophotometer. Thermogravimetric analyses (TGA) and simultaneous differential scanning calorimetry (DSC) measurements were performed in nitrogen flow (40 mL min^{-1}) with a TA instruments SDT Q600 thermal analyzer in the range from 30 to 1000 °C with a heating rate of 10 °C min^{-1}. Triplicate TGA and DSC runs have been performed to ensure reproducibility.

Surface morphology was investigated on a selected piece of nanocomposite considered to be representative of the material. A FESEM Zeiss Σigma 300 VP (Zeiss Oberkochen, Germany) equipped with an energy dispersive spectrometer (EDS) C-MaxN SDD (Oxford Instruments, Oxford, U.K.) with an active area of 20 mm^2 (Oxford Instruments, Oxford, U.K.) was used to perform analysis on the selected samples. The EDS spectrometer was calibrated using MAC standards (Micro-Analysis Consultants Ltd., United Kingdom) for elemental analysis. TEM analyses were performed with an FEI Tecnai 12 instrument (120 kV; filament: LaB6), by dropping 20 lL of 1 g/L powder suspensions in water on Formvar-coated Cu grid (300 mesh, Agar Scientific, Stansted, UK). The microscope was calibrated by using the S106 Cross Grating (Agar Scientific, Stansted, UK). Alignments and astigmatism correction were carried out following the factory settings and fast Fourier transform processing, respectively.

X-ray powder diffraction (XRD) analysis were carried out on the synthetized samples using a Miniflex II (Rigaku Corporation, Tokyo, Japan) diffractometer equipped with Cu tube (Cu-Kα) working at 15 mA and 30 kV. Since the amount of synthetized sample was very small, NaF powder (Mallinckrodt Baker B.V., Holland) was pressed inside the sample holder. Then, the synthetized sample was ground in an agate mortar, placed at the center of the NaF substrate and pressed to have a flat surface. XRD data acquisitions were carried out in the range 3–70° 2θ (step width of 0.02° 2θ, counting time 3 s/step) using a Soller slit of 0.3 mm, a divergent slit of 1.25°, a mask of 10 mm and an antiscatter slit of 1.25°. XRD patterns performed for pure NaF, CeO_2, Fe_3O_4, cerium (III) oxalate hydrate and iron (II) oxalate dihydrate (humboltite) have been reported in the references listed in Table S1.

3.2. Synthesis of Magnetite-Ceria Nanocomposites

There are two steps to synthesize the magnetically recoverable magnetite-ceria nanoparticles: the synthesis of Fe_3O_4 nanoparticles, followed by nanoceria formation.

3.2.1. Synthesis of Fe_3O_4 Nanoparticles

Magnetite nanoparticles were prepared by a hydrothermal synthesis assisted by microwave irradiation using $FeCl_2 \cdot 4H_2O$ as precursor and hydrated hydrazine in alkaline condition as oxidant agent, as reported in ref. [36]. The nano powders obtained by microwave-assisted synthesis were labeled as Fe_3O_4, when no additive was used, and as Fe_3O_4:PVP, Fe_3O_4:CITR and Fe_3O_4:OA when polyvinylpyrrolidone, trisodium citrate dihydrate or oleic acid were used as additives during synthesis, respectively.

3.2.2. Coating of Fe_3O_4 Nanoparticles with Ceria

In a typical reaction, Fe_3O_4 (0.1000 g, 0.432 mmol) and $(NH_4)_2Ce(NO_3)_6$ (0. 3534 g, 0.645 mmol, Ce/Fe_3O_4 molar ratio = 1.5) were mixed in ethylene glycol (15 mL) in a 100 mL Teflon®autoclave. The Teflon® autoclave was then sealed and placed in the microwave applicator using 2.45 GHz frequency with a maximum power of 1000 W. The microwave power was adjusted to reach the settled temperature of 200 °C in 10 min with a dwell time of 45 min. The temperature was monitored by means of a direct optic fiber temperature sensor inserted in a thermowell of the reference vessel. After reaction, the vessel was cooled down to room temperature by means of ventilation applied to the vessels inside the microwave applicator. The as-obtained dark suspension was centrifuged and washed with water (3 × 5 mL) and acetone (5 mL), and a black powder was finally obtained after drying in oven at 80 °C overnight. Yield = 83%, m = 174.7 mg. This nanomaterial was labeled as $Fe_3O_4/1.5CeO_2$, to specify that the Ce/Fe_3O_4 molar ratio used during synthesis was 1.5.

Similarly, by employing Fe_3O_4:PVP (0.1000 g, 0.432 mmol), Fe_3O_4:CITR (0.1000 g, 0.432 mmol) and Fe_3O_4:OA (0.1000 g, 0.432 mmol), respectively as seeds instead of Fe_3O_4, and by using the above mentioned procedure, the following nanomaterials were obtained: Fe_3O_4:PVP/$1.5CeO_2$ (Yield = 82%, m = 172.4 mg), Fe_3O_4:CITR/$1.5CeO_2$ (Yield = 90%, m = 190.4 mg) and Fe_3O_4:OA/$1.5CeO_2$ (Yield = 60%, m = 126.7 mg).

The same procedure was repeated by using Fe_3O_4 (0.1000 g, 0.432 mmol) or Fe_3O_4:PVP (0.1000 g, 0.432 mmol) or Fe_3O_4:CITR (0.1000 g, 0.432 mmol) or Fe_3O_4:OA (0.1000 g, 0.432 mmol) in the presence of $(NH_4)_2Ce(NO_3)_6$ (0.1413 g, 0.258 mmol, Ce/Fe_3O_4 molar ratio = 0.6), yielding $Fe_3O_4/0.6CeO_2$ (Yield = 64%, m = 128.4 mg), Fe_3O_4:PVP/$0.6CeO_2$ (Yield = 61%, m = 122.4 mg), Fe_3O_4:CITR/$0.6CeO_2$ (Yield = 61%, m = 127.0 mg) and Fe_3O_4:OA/$0.6CeO_2$ (Yield = 29%, m = 110.6 mg), respectively.

3.3. Synthesis of Ceria Nanoparticles $1.5CeO_2$ and $0.6CeO_2$

For comparison purposes, pure CeO_2 nanoparticles were also prepared by the microwave-assisted solvothermal method in the same conditions reported in the previous paragraph, but in the absence of magnetite seeds, yielding $1.5CeO_2$ and $0.6CeO_2$, respectively. Ceria nanoparticles were, thus, prepared by a solvothermal synthesis assisted by microwave irradiation using $(NH_4)_2Ce(NO_3)_6$ as precursor. In the general procedure, a solution was prepared dissolving $(NH_4)_2Ce(NO_3)_6$ (0.3534 g, 0.645 mmol or 0.1413 g, 0.258 mmol, for the synthesis of $1.5CeO_2$ or $0.6CeO_2$, respectively) in ethylene glycol (15 mL) in a 100 mL Teflon® autoclave. The same procedure described above was used for the microwave treatment.

$0.6CeO_2$: yield = 48%, m = 21.2 mg.

$1.5CeO_2$: yield = 76%, m = 84.1 mg.

3.4. Catalytic Experiments

Benzyl alcohol (21.6 mg, 0.2 mmol) and aniline (37.3 mg, 0.4 mmol) were put in a glass tube under air without solvent. Then, the appropriate amount of catalyst (containing in any case 10 mg of CeO_2) was added and stirred vigorously at 50 °C for 3h. Afterwards, the reaction mixture was cooled to room temperature and added of the internal standard (diphenyl, 10 mg) for conversion assessment and ethanol (2 mL). The catalyst was pushed to the bottom of the tube with the help of an external magnet and the liquid solution was transferred to a new vial. The catalyst was then washed with ethanol (3 × 1 mL) and the washing liquors were collected and added to the reaction solution for GLC analyses. In order to compare catalytic results with those obtained by other researchers, the reaction rates were used to assess the catalytic ability, by calculating the imine formation amount per hour per catalyst amount (mmol $h^{-1}g^{-1}$).

3.5. Reusing of the Catalyst

The catalyst removed from the reaction solution was dried in oven at 80 °C overnight and then calcinated at 400 °C for 1 h under air, before being employed for a subsequent catalytic run.

4. Conclusions

A microwave-assisted solvothermal procedure in ethylene glycol was proposed to prepare magnetite/ceria nanocomposites by depositing nanoceria on magnetite seeds of different morphologies (hexagonal, spheroidal, quasi-spherical), using 0.6 and 1.5 Ce/Fe_3O_4 molar ratio during synthesis. IR, XRD, TEM and TGA/DSC analyses suggested: (*i*) to calcinate the new materials at 550 °C for avoiding sintering processes and promoting the ceria transition phase from amorphous to crystalline state; and (*ii*) to use at least 1.5 Ce/Fe_3O_4 molar ratio during preparation for obtaining a more stable magnetite/ceria nanostructure. Thus, the new nanocomposites synthetized with 1.5 Ce/Fe_3O_4 molar ratio and calcined at 550 °C were carefully investigated by IR, XRD, FESEM, EDS and TEM analyses. The Fe_3O_4 nanoparticles kept their pristine morphology even after ceria deposition and subsequent calcination at 550 °C. All nanocomposites resulted magnetically active, thus easily removable from the reaction mixture with the help of an external magnet. The synthetized nanomaterials were tested as catalysts for imine formation from benzyl alcohol and aniline in the absence of any solvent under air. The highest imine conversion rate was obtained with Fe_3O_4/CeO_2, prepared in the absence of any organic stabilizer. Its catalytic activity was even higher than commercial nanoceria. The new catalyst was recyclable for at least five runs. Its catalytic activity increased with the reuses probably because the organic impurities coming from the solvothermal synthesis depleted over the runs, as suggested by XRD analyses, rendering the whole system highly interesting in the field of nano-catalysis.

Supplementary Materials: The following are available online at http://www.mdpi.com/2073-4344/10/11/1325/s1, Figure S1: TGA (black) and DSC (grey) curves for a) 0.6CeO2 and b) 1.5CeO2, Figure S2: IR spectra of a) 0.6CeO2 and b) 1.5CeO2 as prepared (black) and after calcination at 1000 °C (grey), Figure S3: TEM images of a) Fe3O4/0.6CeO2, b) Fe3O4/1.5CeO2, both after calcination at 1000 °C, Figure S3: TEM images of a) Fe3O4/0.6CeO2, b) Fe3O4/1.5CeO2, both after calcination at 1000 °C, Figure S5: EDS analysis of Fe3O4:CITR/1.5CeO2 after calcination at 550 °C, Figure S6: EDS analysis of Fe3O4:PVP/1.5CeO2 after calcination at 550 °C, Figure S7: EDS analysis of Fe3O4:OA/1.5CeO2 after calcination at 550 °C, Figure S8: FT-IR spectrum of Fe3O4/1.5CeO2 after calcination for 3 h at 400 °C, Table S1: References reporting XRD patterns of pure listed compounds, Table S2: Imine synthesis from benzyl alcohol and aniline over various catalysts.

Author Contributions: Conceptualization: A.R. and M.M.D.; Data Curation: M.M.D.; Formal Analysis: N.C.; Funding Acquisition: P.M.; Investigation: A.R., M.C.D. and M.M.D.; Methodology: M.C.D. and M.M.D.; Resources: P.M.; Software: I.A. and R.T.; Validation: I.A., R.T., M.M., G.R. and A.N.; Writing—Original Draft Preparation: M.M.D.; Writing—Review & Editing: M.M.D. and A.R.; Visualization: M.M., G.R. and A.N.; Supervision: M.M.D.; Project Administration: M.M.D. All authors have read and agreed to the published version of the manuscript.

Funding: This research was supported by Politecnico di Bari (Italy) with Fondi di Ricerca di Ateneo, FRA2016.

Acknowledgments: We Thank A. Boghetich (MicroXRayLab, Politecnico di Bari) for his kind assistance in SEM analyses.

Conflicts of Interest: The authors declare no conflict of interest. The funders had no role in the design of the study; in the collection, analyses or interpretation of data; in the writing of the manuscript or in the decision to publish the results.

References

1. Trovarelli, A. Catalytic Properties of Ceria and CeO_2-Containing Materials. *Catal. Rev.* **1996**, *38*, 439–520. [CrossRef]
2. Zhang, B.; Zhang, S.-G.; Liu, B. Effect of oxygen vacancies on ceria catalyst for selective catalytic reduction of NO with NH3. *Appl. Surf. Sci.* **2020**, *529*, 147068. [CrossRef]
3. RajeshKumar, S.; Naik, P. Synthesis and biomedical applications of Cerium oxide nanoparticles—A Review. *Biotechnol. Rep.* **2018**, *17*, 1–5. [CrossRef] [PubMed]
4. Kargozar, S.; Baino, F.; Hoseini, S.J.; Hamzehlou, S.; Darroudi, M.; Verdi, J.; Hasanzadeh, L.; Kim, H.-W.; Mozafari, M. Biomedical applications of nanoceria: New roles for an old player. *Nanomedicine* **2018**, *13*, 3051–3069. [CrossRef] [PubMed]

5. Xu, C.; Qu, X. Cerium oxide nanoparticle: A remarkably versatile rare earth nanomaterial for biological applications. *NPG Asia Mater.* **2014**, *6*, e90. [CrossRef]
6. Jasinski, P.; Suzuki, T.; Anderson, H.U. Nanocrystalline undoped ceria oxygen sensor. *Sens. Actuators B Chem.* **2003**, *95*, 73–77. [CrossRef]
7. Montini, T.; Melchionna, M.; Monai, M.; Fornasiero, P. Fundamentals and Catalytic Applications of CeO2-Based Materials. *Chem. Rev.* **2016**, *116*, 5987–6041. [CrossRef]
8. Haeussler, A.; Abanades, S.; Julbe, A.; Jouannaux, J.; Cartoixa, B. Solar thermochemical fuel production from H_2O and CO_2 splitting via two-step redox cycling of reticulated porous ceria structures integrated in a monolithic cavity-type reactor. *Energy* **2020**, *201*, 117649. [CrossRef]
9. Goubin, F.; Rocquefelte, X.; Whangbo, M.; Montardi, Y.; Brec, R.; Jobic, S. Experimental and Theoretical Characterization of the Optical Properties of CeO_2, $SrCeO_3$, and Sr_2CeO_4 Containing Ce^{4+} (f0). *Ions. Chem. Mater.* **2004**, *16*, 662–669. [CrossRef]
10. Dhall, A.; Self, W.T. Cerium Oxide Nanoparticles: A Brief Review of Their Synthesis Methods and Biomedical Applications. *Antioxidants* **2018**, *7*, 97. [CrossRef]
11. Thakur, N.; Manna, P.; Das, J. Synthesis and biomedical applications of nanoceria, a redox active nanoparticle. *J. Nanobiotechnol.* **2019**, *17*, 1–27. [CrossRef] [PubMed]
12. Naz, S.; Beach, J.; Heckert, B.; Tummala, T.; Pashchenko, O.; Banerjee, T.; Santra, S. Cerium oxide nanoparticles: A 'radical' approach to neurodegenerative disease treatment. *Nanomedicine* **2017**, *12*, 545–553. [CrossRef] [PubMed]
13. Maqbool, Q.; Nazar, M.; Naz, S.; Hussain, T.; Jabeen, N.; Kausar, R.; Anwaar, S.; Abbas, F.; Jan, T. Antimicrobial potential of green synthesized CeO_2 nanoparticles from Olea europaea leaf extract. *Int. J. Nanomed.* **2016**, *11*, 5015–5025. [CrossRef] [PubMed]
14. Zhang, Y.; Wu, X.; Hou, C.; Shang, K.; Yang, K.; Tian, Z.; Pei, Z.; Qu, Y.; Pei, Y. Dual-responsive dithio-polydopamine coated porous CeO_2 nanorods for targeted and synergistic drug delivery. *Int. J. Nanomed.* **2018**, *13*, 2161–2173. [CrossRef]
15. Huang, X.; Li, L.; Li, G. Synthesis of CeO_2 assemblies through interaction with short-chain dicarboxylic acids under facile hydrothermal conditions. *RSC Adv.* **2019**, *9*, 28581–28587. [CrossRef]
16. Zhang, H.; He, X.; Zhang, Z.; Zhang, P.; Li, Y.; Ma, Y.; Kuang, Y.; Zhao, Y.; Chai, Z. Nano-CeO2Exhibits Adverse Effects at Environmental Relevant Concentrations. *Environ. Sci. Technol.* **2011**, *45*, 3725–3730. [CrossRef]
17. Fisher, T.J.; Wang, M.; Ibrahim, Y.; Steffensmeier, B.; Cheung, C.L. Effect of sodium nitrate on microwave-assisted synthesis of ceria nanocubes. *Mater. Lett.* **2016**, *178*, 71–74. [CrossRef]
18. Panda, S.R.; Singh, R.K.; Priyadarshini, B.; Rath, P.P.; Parhi, P.; Sahoo, T.; Mandal, D.; Sahoo, T.R. Nanoceria: A rare-earth nanoparticle as a promising anti-cancer therapeutic agent in colon cancer. *Mater. Sci. Semicond. Process.* **2019**, *104*, 104669. [CrossRef]
19. Xu, H.; Zeiger, B.W.; Suslick, K.S. Sonochemical synthesis of nanomaterials. *Chem. Soc. Rev.* **2013**, *42*, 2555–2567. [CrossRef]
20. Wu, K.; Sun, L.-D.; Yan, C.-H. Ceria-Based Nanocatalysts: Recent Progress in Well-Controlled Synthesis of Ceria-Based Nanocatalysts towards Enhanced Catalytic Performance. *Adv. Energy Mater.* **2016**, *6*, 1600501. [CrossRef]
21. Gao, X.; Chen, C.; Ren, S.; Zhang, J.; Su, D. Structural Effects of Cerium Oxides on Their Thermal Stability and Catalytic Performance in Propane Oxidation Dehydrogenation. *Chin. J. Catal.* **2012**, *33*, 1069–1074. [CrossRef]
22. Trovarelli, A.; Llorca, J. Ceria Catalysts at Nanoscale: How Do Crystal Shapes Shape Catalysis? *ACS Catal.* **2017**, *7*, 4716–4735. [CrossRef]
23. Toyao, T.; Rashed, N.; Morita, Y.; Kamachi, T.; Siddiki, S.H.; Ali, A.; Touchy, A.S.; Kon, K.; Maeno, Z.; Yoshizawa, K.; et al. Esterification of Tertiary Amides by Alcohols Through C−N Bond Cleavage over CeO 2. *ChemCatChem* **2019**, *11*, 449–456. [CrossRef]
24. Kim, D.; Kwon, H.J.; Hyeon, T. Magnetite/Ceria Nanoparticle Assemblies for Extracorporeal Cleansing of Amyloid-β in Alzheimer's Disease. *Adv. Mater.* **2019**, *31*, 1807965. [CrossRef] [PubMed]
25. Gu, Z.; Li, K.; Qing, S.; Zhu, X.; Wei, Y.; Li, Y.; Wang, H. Enhanced reducibility and redox stability of Fe2O3 in the presence of CeO2 nanoparticles. *RSC Adv.* **2014**, *4*, 47191–47199. [CrossRef]

26. Rashid, J.; Parveen, N.; Haq, T.; Iqbal, A.; Talib, S.H.; Awan, S.U.; Hussain, N.; Zaheer, M. g-C3N4/CeO2/Fe3O4 Ternary Composite as an Efficient Bifunctional Catalyst for Overall Water Splitting. *ChemCatChem* **2018**, *10*, 5587–5592. [CrossRef]
27. Gogoi, A.; Navgire, M.; Sarma, K.C.; Gogoi, P. Fe_3O_4 -CeO_2 metal oxide nanocomposite as a Fenton-like heterogeneous catalyst for degradation of catechol. *Chem. Eng. J.* **2017**, *311*, 153–162. [CrossRef]
28. Farokhi, M.; Parvareh, A.; Moraveji, M.K. Performance of ceria/iron oxide nano-composites based on chitosan as an effective adsorbent for removal of Cr(VI) and Co(II) ions from aqueous systems. *Environ. Sci. Pollut. Res.* **2018**, *25*, 27059–27073. [CrossRef]
29. Khataee, A.; Hassandoost, R.; Pouran, S.R. Cerium-substituted magnetite: Fabrication, characterization and sonocatalytic activity assessment. *Ultrason. Sonochemistry* **2018**, *41*, 626–640. [CrossRef]
30. Zhang, F.; Yao, S.; Liu, Z.; Gutiérrez, R.A.; Vovchok, D.; Cen, J.; Xu, W.; Ramírez, P.J.; Kim, T.; Senanayake, S.D.; et al. Reaction of Methane with MOx/CeO_2 (M = Fe, Ni, and Cu) Catalysts: In Situ Studies with Time-Resolved X-ray Diffraction. *J. Phys. Chem. C* **2018**, *122*, 28739–28747. [CrossRef]
31. Dai, Q.; Wang, J.; Yu, J.; Chen, J.; Chen, J. Catalytic ozonation for the degradation of acetylsalicylic acid in aqueous solution by magnetic CeO_2 nanometer catalyst particles. *Appl. Catal. B Environ.* **2014**, *144*, 686–693. [CrossRef]
32. Wei, J.; Yao, H.; Wang, Y.; Luo, G. Controllable Preparation and Catalytic Performance of Magnetic Fe_3O_4@CeO_2-Polysulfone Nanocomposites with Core–Shell Structure. *Ind. Eng. Chem. Res.* **2018**, *57*, 15039–15045. [CrossRef]
33. Wu, Y.; Yang, Y.; Zhao, W.; Xu, Z.P.; Little, P.J.; Whittaker, A.K.; Zhang, R.; Ta, H.T. Novel iron oxide-cerium oxide core-shell nanoparticles as a potential theranostic material for ROS related inflammatory diseases. *J. Mater. Chem. B* **2018**, *6*, 4937–4951. [CrossRef] [PubMed]
34. Vono, L.L.R.; Damasceno, C.C.; Matos, J.R.; Jardim, R.F.; Landers, R.; Masunaga, S.H.; Rossi, L.M. Separation technology meets green chemistry: Development of magnetically recoverable catalyst supports containing silica, ceria, and titania. *Pure Appl. Chem.* **2018**, *90*, 133–141. [CrossRef]
35. Gawande, M.B.; Bonifácio, V.D.B.; Varma, R.S.; Nogueira, I.D.; Bundaleski, N.; Ghumman, C.A.A.; Teodoro, O.M.N.D.; Branco, P.S. Magnetically recyclable magnetite–ceria (Nanocat-Fe-Ce) nanocatalyst–applications in multicomponent reactions under benign conditions. *Green Chem.* **2013**, *15*, 1226–1231. [CrossRef]
36. Rizzuti, A.; Dassisti, M.; Mastrorilli, P.; Sportelli, M.C.; Cioffi, N.; Picca, R.A.; Agostinelli, E.; Varvaro, G.; Caliandro, R. Shape-control by microwave-assisted hydrothermal method for the synthesis of magnetite nanoparticles using organic additives. *J. Nanopart. Res.* **2015**, *17*, 1–16. [CrossRef]
37. Tamura, M.; Tomishige, K. Redox Properties of CeO_2 at Low Temperature: The Direct Synthesis of Imines from Alcohol and Amine. *Angew. Chem. Int. Ed.* **2015**, *54*, 864–867. [CrossRef]
38. Zhang, J.; Yang, J.; Wang, J.; Ding, H.; Liu, Q.; Schubert, U.; Rui, Y.; Xu, J. Surface oxygen vacancies dominated CeO_2 as efficient catalyst for imine synthesis: Influences of different cerium precursors. *Mol. Catal.* **2017**, *443*, 131–138. [CrossRef]
39. Hirano, M.; Kato, E. Hydrothermal Synthesis of Cerium(IV) Oxide. *J. Am. Ceram. Soc.* **2005**, *79*, 777–780. [CrossRef]
40. Leonelli, C.; Lojkowski, W. Main development directions in the application of microwave irradiation to the synthesis of nanopowders. *Chem. Today* **2007**, *25*, 34–38.
41. De Almeida, L.; Grandjean, S.; Vigier, N.; Patisson, F. Insights into the Thermal Decomposition of Lanthanide(III) and Actinide(III) Oxalates—From Neodymium and Cerium to Plutonium. *Eur. J. Inorg. Chem.* **2012**, *31*, 4986–4999. [CrossRef]
42. Lundberg, M.; Skårman, B.; Cesar, F.; Wallenberg, L.R. Mesoporous thin films of high-surface-area crystalline cerium dioxide. *Microporous Mesoporous Mater.* **2002**, *54*, 97–103. [CrossRef]
43. Ma, M.; Zhang, Y.; Yu, W.; Shen, H.; Zhang, H.; Gu, N. Preparation and characterization of magnetite nanoparticles coated by amino silane. *Colloids Surf. A Physicochem. Eng. Asp.* **2003**, *212*, 219–226. [CrossRef]
44. El Desouky, F.G.; Saadeldin, M.; Mahdy, M.A.; El Wahab, S.A.; El Zawawi, I. Impact of calcination temperature on the structure, optical and photoluminescence properties of NanocrystallineCerium oxide thin films. *Mater. Sci. Semicond. Process.* **2020**, *111*, 104991. [CrossRef]
45. Prakash, S. Reduction and sintering of fluxed iron ore pellets-a comprehensive review. *J. South Afr. Inst. Min. Metall.* **1996**, *96*, 3–16.

46. Moloto, L.H.; Manzini, S.S.; Dikio, E.D. Reduction of Magnetite in the Presence of Activated Carbon Using Mechanical Alloying. *J. Chem.* **2013**, *2013*, 1–8. [CrossRef]
47. Wang, S.; Zhang, P. Adsorption and dissociation of H2O monomer on ceria(111): Density functional theory calculations. *Mod. Phys. Lett. B* **2020**, *34*, 2050254. [CrossRef]

Publisher's Note: MDPI stays neutral with regard to jurisdictional claims in published maps and institutional affiliations.

© 2020 by the authors. Licensee MDPI, Basel, Switzerland. This article is an open access article distributed under the terms and conditions of the Creative Commons Attribution (CC BY) license (http://creativecommons.org/licenses/by/4.0/).